

Charged-current non-standard neutrino interactions at the LHC and HL-LHC

Chong-Xing Yue^{1,2,*}, Xue-Jia Cheng^{1,2,†} and Ji-Chong Yang^{1,2,‡}

¹*Department of Physics, Liaoning Normal University, Dalian 116029, China*

²*Center for Theoretical and Experimental High Energy Physics,*

Liaoning Normal University, Dalian 116029, China

(Dated: March 2, 2023)

Abstract

A series of new physics scenarios predict the existence of the extra charged gauge boson W' , which can induce charged-current (CC) non-standard neutrino interactions (NSIs). The theoretical constraints on the simplified W' model and further on the CC NSI parameters $\tilde{\epsilon}_{\alpha\beta}^{qq'Y}$ from partial wave unitarity and W' decays are considered. The sensitivity of the process $pp \rightarrow W' \rightarrow \ell\nu$ to the W' model at the LHC and high-luminosity (HL) LHC experiments is investigated by estimating the expected constraints on $\tilde{\epsilon}_{\alpha\beta}^{qq'Y}$ ($\alpha = \beta = e$ or μ) using a Monte-Carlo (MC) simulation. We find that the interference effect plays an important role, and the LHC can strongly constrain $\tilde{\epsilon}_{\alpha\beta}^{qq'L}$. Compared with those at the 13 TeV LHC with $\mathcal{L} = 139 \text{ fb}^{-1}$, the expected constraints at the 14 TeV LHC with $\mathcal{L} = 3 \text{ ab}^{-1}$ can be strengthened to approximately one order of magnitude.

* cxyue@lnnu.edu.cn

† cxj225588@163.com

‡ yangjichong@lnmu.edu.cn

I. INTRODUCTION

The Standard Model (SM) has achieved great success in describing elementary particles and interactions. Numerous experimental studies have verified its predictions with very high accuracy. However, the SM does not reveal the origin of the neutrino mass. Strong evidence show that neutrinos with different flavors cannot oscillate with each other without small mass differences. The origin of neutrino mass requires new physics beyond the SM (BSM) [1, 2], many examples of which share the common feature of emerging effective non-standard neutrino interactions (NSIs) between neutrinos and matter fields [3–7]. NSIs are generally divided into two types: the neutral-current (NC) NSI and charged-current (CC) NSI. The NC NSI mainly affects neutrino propagation in matter, whereas the CC NSI is associated with neutrino production and detection processes (for recent reviews, see Refs. [5–8]). These new interactions lead to rich phenomenology in neutrino oscillation experiments and high- and low-energy collider experiments. Very strong constraints on the NSIs have been obtained, see, for example, Refs. [4, 9–18]. The experiments generally impose more strict restrictions on the CC NSI than on the NC NSI [19, 20].

Recently, numerous phenomenological studies have been conducted on NSIs. For example, the new gauge boson Z' can introduce NC NSIs [12, 21–26]. Refs. [12, 24–26] studied the constraints on NC NSIs in the context of a simplified Z' model using mono-jet signals at the Large Hadron Collider (LHC). Many BSMs predict the existence of W' , such as the left-right symmetry model [27, 28], little Higgs models [29], and models with extra dimensions [30, 31], which can lead to CC NSIs. Previous searches for the W' boson at the LHC have been carried out by the ATLAS and CMS collaborations with data collected at the center-of-mass (c. m.) energy $\sqrt{s} = 7$ TeV [32, 33], 8 TeV [34, 35], and 13 TeV [36, 37]. The most sensitive channels are $e\nu$ and $\mu\nu$ production, with the constraints to date set in Refs. [38, 39], which can be translated to constraints on CC NSIs. The LHC experiments have further promoted the theoretical research on W' properties [40–42]. Although there are other new particles that can also cause the CC NSI, such as charged scalar particles (for example, see [14]), in this paper, we focus on the simplified W' model.

It has been shown that there is a well-known ‘degeneracy’ between the parameter spaces of NSIs in neutrino oscillation experiments because the effects of NSIs strongly depend on the flavor structure and oscillation channel being studied [43]. Although it is difficult to

break the degeneracy at neutrino facilities, the LHC plays a complementary role in the study of NSIs [4, 11, 14, 44], and it is believed to be able to break the degeneracy because the effects of NSIs at the LHC do not distinguish between different neutrino flavors [25, 26]. Furthermore, the LHC is sensitive to both vector- and axial-vector interactions, whereas neutrino oscillation experiments are not sensitive to the latter.

Thus far, various studies have been completed on the detection of W' at the LHC, and searching for this type of new particle will continue to be important at the future LHC with higher luminosities (HL-LHC). Based on a Monte-Carlo (MC) simulation, the expected constraints on the CC NSI parameters via the process $pp \rightarrow \ell^+ \nu_\ell$ are studied with an emphasis on the effects of the interference between the CC NSI and the SM. Moreover, the sensitivities at future runs of the LHC are also discussed.

The remainder of this paper is organized as follows: In Sec. II, we consider the theoretical constraints on the simplified W' model and further on the CC NSI parameters $\tilde{\epsilon}_{\alpha\beta}^{qq'Y}$ ($\alpha = \beta = e$ or μ) in terms of partial wave unitarity and W' decay. The sensitivities of the process $pp \rightarrow \ell^+ \nu_\ell$ to the parameters $\tilde{\epsilon}_{\alpha\beta}^{udY}$ at the current LHC and future runs of the LHC are studied in Secs. III and IV, respectively. Our conclusions and discussions are given in Sec. V.

II. THEORETICAL CONSTRAINTS ON THE SIMPLIFIED W' MODEL AND NSI PARAMETERS

NSIs are new vector interactions between neutrinos and matter fields, induced by either a vector or scalar mediator. They can be parameterized in terms of the low-energy effective four-fermion Lagrangian [19, 20, 44, 45]. CC NSIs with quarks are given by the effective Lagrangian

$$\mathcal{L}_{NSI,CC} = -2\sqrt{2}G_F\epsilon_{\alpha\beta}^{qq'Y} [\bar{q}\gamma^\mu P_Y q'] [\bar{\nu}_\alpha\gamma_\mu P_L \ell_\beta] + h.c., \quad (1)$$

where G_F is the Fermi constant, α and β are lepton flavor indices, $\alpha, \beta \in \{e, \mu, \tau\}$, and P_Y is a chiral projection operator (P_L or P_R). We assume that there are only left-handed neutrinos in the above equation. The parameters $\epsilon_{\alpha\beta}^{qq'Y}$ are dimensionless coefficients that quantify the strengths of the new vector interactions. According to Hermiticity, $\epsilon_{\alpha\beta}^{qq'Y} = \epsilon_{\beta\alpha}^{qq'Y*}$. The CC NSI might change the production of neutrinos through its effects on processes such as muon decay and inverse beta decay [46, 47].

Because the momentum transfer can be very high to resolve further dynamics of new

physics at the LHC, the influence of the CC NSI may not be simply described by the effective operators. In this paper, we focus on a simplified model with the CC NSI induced by the exchange of a W' boson. The effective Lagrangian can be written as [48–50]

$$\mathcal{L}_{W'} = -\frac{g}{\sqrt{2}} \left[V_{qq'} \bar{q} \gamma^\mu \left(A_L^{qq'} P_L + A_R^{qq'} P_R \right) q' + B_L^{\alpha\beta} \bar{\ell}_\alpha \gamma^\mu P_L \nu_\beta \right] W'_\mu + h.c., \quad (2)$$

where W'_μ denotes the new force carrier with a mass $M_{W'}$, and g is the electroweak coupling constant. $q = \{u, c, t\}$ and $q' = \{d, s, b\}$ are up-type and down-type quarks, respectively. $V_{qq'}$ is the Cabibbo-Kobayashi-Maskawa (CKM) matrix element, in which the non-diagonal terms contribute to flavor changing neutral current (FCNC) processes [51], and the contributions are very small and negligible. For simplicity, one can also absorb $gV_{qq'}/\sqrt{2}$ into the coupling parameters $A_Y^{qq'}$ and $B_L^{\alpha\beta}$.

In a simplified model framework, the relationship between Eq. (1) and Eq. (2) can be thought of as $\epsilon_{\alpha\beta}^{qq'Y} \sim g_X^2/M_X^2$, with X representing a charged mediator. Because the Wilson coefficients of an effective field theory (EFT) are typically functions of energy scales, Eq. (2) implies a substitution of $\epsilon_{\alpha\beta}^{qq'Y}$ in Eq. (1), $\epsilon_{\alpha\beta}^{qq'Y} \rightarrow \epsilon_{\alpha\beta}^{qq'Y}(s)$, with $\epsilon_{\alpha\beta}^{qq'Y}(s) = -M_{W'}^2 \tilde{\epsilon}_{\alpha\beta}^{qq'Y} / (s - M_{W'}^2)$, and $\epsilon_{\alpha\beta}^{qq'Y} = \tilde{\epsilon}_{\alpha\beta}^{qq'Y}$ when $s \rightarrow 0$, and

$$\tilde{\epsilon}_{\alpha\beta}^{qq'L} = A_L^{qq'} B_L^{\beta\alpha*} \left(\frac{M_W}{M_{W'}} \right)^2, \quad \tilde{\epsilon}_{\alpha\beta}^{qq'R} = A_R^{qq'} B_L^{\beta\alpha*} \left(\frac{M_W}{M_{W'}} \right)^2. \quad (3)$$

However, it can also be considered that the effective operator in Eq. (1) corresponds to the leading order of expansion of $\epsilon_{\alpha\beta}^{qq'Y}(s)$ in $s/M_{W'}^2$, whereas Eq. (2) also collects the contributions of the higher dimensional operators corresponding to the higher orders of $s/M_{W'}^2$.

In principle, there are also flavor violating NSI couplings. Neutrino oscillation and scattering experiments are found to have tight constraints on diagonal NSIs, whereas off-diagonal NSIs are primarily constrained by various low-energy processes, such as atomic parity violation and charged-lepton flavor violation (cLFV) [14]. Because only diagonal NSIs are relevant for the process $pp \rightarrow \ell\nu$, we concentrate on the $\alpha = \beta$ case in this paper.

A. Unitarity constraints from the $f\bar{f} \rightarrow V_1 V_2$ process

In a weakly coupled renormalizable theory, the high-energy behavior of the scattering amplitude of bosons under the perturbation calculation is expected to respect unitarity. It has been shown that the constraint on $M_{Z'}$ can be obtained using partial wave unitarity

bounds derived from the $f\bar{f} \rightarrow V_1 V_2$ process, where V represents vector bosons, including SM W, Z bosons and also the new gauge bosons W', Z' , and f and \bar{f} are fermions and anti-fermions [52]. The helicity amplitudes can be expanded as [53, 54]

$$\mathcal{M}_{f\sigma_1 \bar{f}\sigma_2 \rightarrow V_1, \lambda_3 V_2, \lambda_4} = 16\pi \sum_J \left(J + \frac{1}{2} \right) \delta_{\sigma_1, -\sigma_2} e^{i(m_1 - m_2)\phi} d_{m_1, m_2}^J(\theta, \phi) T_J, \quad (4)$$

where $m_1 = \sigma_1 - \sigma_2$ and $m_2 = \lambda_3 - \lambda_4$ are the helicity differences of fermions and vector bosons, respectively. d_{m_1, m_2}^J are Wigner d -functions [53], ϕ and θ are the azimuth and zenith angles of V_1 in the rest frame of the fermions whose Z -axis points in the direction of f . The partial wave unitarity bound is $|T_J| \leq 1$ [55, 56], where T_J is the coefficient of partial wave expansion. As noted in Ref. [52], we only need to consider processes with the longitudinal final states $f_{\pm\frac{1}{2}} \bar{f}_{\pm\frac{1}{2}} \rightarrow V_{1, \lambda_3=0} V_{2, \lambda_4=0}$, whose amplitudes are denoted as $\mathcal{M}_{f_1 \bar{f}_2 \rightarrow V_1 V_2}^{(-+)}$ and $\mathcal{M}_{f_1 \bar{f}_2 \rightarrow V_1 V_2}^{(+-)}$, where ‘ $-+$ ’ in superscript means $f_{-\frac{1}{2}} \bar{f}_{+\frac{1}{2}}$, and ‘ $+ -$ ’ means $f_{+\frac{1}{2}} \bar{f}_{-\frac{1}{2}}$. In the following, we only consider tree-level processes, including t-channel, u-channel, and s-channel processes. The corresponding Feynman diagrams are shown in Fig. 1. There is also an s-channel scalar exchange diagram, which only contributes to $\mathcal{M}_{f_1 \bar{f}_2 \rightarrow V_1 V_2}^{(++)}$ and $\mathcal{M}_{f_1 \bar{f}_2 \rightarrow V_1 V_2}^{(--)}$; therefore, it is not shown.

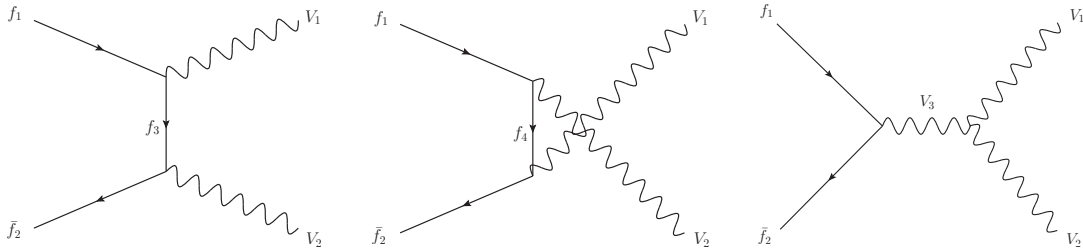


FIG. 1. Tree-level Feynman diagrams of the process $f\bar{f} \rightarrow V_1 V_2$.

$\mathcal{M}_{f_1 \bar{f}_2 \rightarrow V_1 V_2}^{(-+)}$ and $\mathcal{M}_{f_1 \bar{f}_2 \rightarrow V_1 V_2}^{(+-)}$ can be expanded in terms of s as

$$\mathcal{M}_{f_1 \bar{f}_2 \rightarrow V_1 V_2}^{(\pm\mp)} = \mathcal{A}_1 s + \mathcal{A}_0 + \mathcal{A}_{-1} s^{-1} + \mathcal{A}_{-2} s^{-2} + \dots \quad (5)$$

Partial wave unitarity should be satisfied for arbitrary s . When $s \rightarrow \infty$, a finite $|T_J|$ implies $\mathcal{A}_1 = 0$, which results in a set of ‘sum rules’ [52, 57],

$$\sum_{f_3} g_{V_1 f_1 \bar{f}_3}^{L/R} g_{V_2 f_3 \bar{f}_2}^{L/R} - \sum_{f_4} g_{V_1 f_4 \bar{f}_2}^{L/R} g_{V_2 f_1 \bar{f}_4}^{L/R} = \sum_{V_3} g_{V_3 f_1 \bar{f}_2}^{L/R} g_{V_1 V_2 V_3}^{L/R}, \quad (6)$$

where $V_{1,2,3}$ and $f_{1,2,3,4}$ are allowed vector bosons and fermions in the Feynman diagrams in Fig. 1, respectively.

For the scattering amplitudes of the process $f_1\bar{f}_2 \rightarrow V_1V_2$, a new gauge boson Z' must have non-zero coupling with fermions and other gauge bosons, and the existence of Z' is necessary to maintain the perturbative unitarity of all amplitudes. Therefore, triple gauge couplings involving Z' and Z' -fermion couplings must be involved in the calculation of the Feynman diagrams shown in Fig. 1. There are enough ‘sum rules’ to solve all unknown couplings of Z' using Eq. (6), that is, the Z' -fermion couplings are automatically fixed when the W' -fermion couplings are fixed [52]. Certainly, the $W - W'$ and $Z - Z'$ mixings would modify the relevant SM couplings slightly, which can affect the amplitudes of the process $f_1\bar{f}_2 \rightarrow V_1V_2$. It has been shown that the correction effect is less than 1% [52, 58]; hence, for simplicity, we neglect it in our calculations. With the help of Eq. (6), the amplitudes corresponding to the Feynman diagrams in Fig. 1 are written as Eq. (A.1).

Using the relationship $|T_J| \leq 1$, one can obtain a constraint on $A_Y^{qq'}$ or $B_L^{\alpha\alpha}$ from each of the above processes. All of these constraints should be satisfied, therefore, we concentrate on the tightest ones, which depend on the free parameters $M_{W'}$ and $M_{Z'}$. In the case of $0.2 \text{ TeV} < M_{Z'} < 2 \text{ TeV}$ [25] and $s \rightarrow \infty$, the tightest bounds on $A_Y^{qq'}$ or $B_L^{\alpha\alpha}$ are given in Eq. (A.2). The relationship between $M_{W'}$ and the coupling parameters according to Eq. (A.2) are shown in Fig. 17. It can be seen that in the wide range of $M_{W'}$, the tightest bound on $A_L^{qq'}$ originates from the process $u\bar{d} (d\bar{u}) \rightarrow W'Z$. Similarly, the tightest bound on $B_L^{\alpha\alpha}$ mainly arises from the process $e^-e^+ \rightarrow W'Z$. For simplicity, we only use the above bounds. For $A_R^{qq'}$, the two tightest bounds (depending on $M_{W'}$) are both considered. Consequently, the perturbative unitarity constraints on the parameters $\tilde{\epsilon}_{\alpha\alpha}^{qq'Y}$ are

$$\begin{aligned} \left| \tilde{\epsilon}_{\alpha\alpha}^{qq'L} \right| &< \frac{1152\pi^2 M_Z^2 M_W^2}{g^4 c_W^2 |V_{qq'}|^2 (2M_{W'}^2 + M_Z^2)^2}, \\ \left| \tilde{\epsilon}_{\alpha\alpha}^{qq'R} \right| &< \min \left\{ \frac{1152\pi^2 M_Z^2 M_W^2}{|V_{qq'}|^2 s_W^2 g^4 (2M_{W'}^2 + M_Z^2)^2}, \right. \\ &\left. \frac{48\sqrt{2}\pi M_Z M_W^2}{g^2 c_W M_{W'} (2M_{W'}^2 + M_Z^2)} \sqrt{\frac{72\sqrt{2}\pi c_W^2 M_{W'}^2 + s_W^2 g^2 |V_{qq'}|^2 (s_W^2 M_Z^2 - M_{Z'}^2)}{3c_W^2 g^2 |V_{qq'}|^2 (4M_{W'}^2 - M_{Z'}^2)}} \right\}. \end{aligned} \quad (7)$$

By using Eq. (1), the unitarity bounds on $\epsilon_{\alpha\alpha}^{qq'Y}$ can be directly obtained from the process $f\bar{f} \rightarrow f\bar{f}$. However, because the W' model corresponds to the substitution $\epsilon_{\alpha\alpha}^{qq'Y} \rightarrow \epsilon_{\alpha\alpha}^{qq'Y}(s)$, where the latter is just the ‘form factor unitarization’ widely used in the study of SM EFT [59–61], that is, unitarity is guaranteed with this substitution; therefore, the unitarity bounds from the process $f\bar{f} \rightarrow f\bar{f}$ are not considered.

B. Constraints from W' decays

From Eq. (2), the total decay width of the W' boson at leading order can be written as

$$\Gamma_{W'} = M_{W'} \left(\frac{g^2}{16\pi} \sum_{q,q'} |V_{qq'}|^2 \left(|A_L^{qq'}|^2 + |A_R^{qq'}|^2 \right) + \frac{g^2}{48\pi} \left(|B_L^{ee}|^2 + |B_L^{\mu\mu}|^2 + |B_L^{\tau\tau}|^2 \right) \right). \quad (8)$$

Without loss of generality, using the case of $A_L^{ud} \neq 0, B_L^{ee} \neq 0$ as an example, when the mass of fermions are negligible compared with $M_{W'}$,

$$\begin{aligned} \frac{\Gamma_{W'}}{M_{W'}} &= \sum_{qq',Y} \frac{g^2 |V_{qq'}|^2}{16\pi} |A_Y^{qq'}|^2 + \frac{g^2}{48\pi} \sum_{\ell} |B_L^{\alpha\alpha}|^2 \geq \frac{g^2 |V_{ud}|^2}{16\pi} |A_L^{ud}|^2 + \frac{g^2}{48\pi} |B_L^{ee}|^2 \\ &= \left(\sqrt{\frac{g^2 |V_{ud}|^2}{16\pi}} A_L^{ud} - \sqrt{\frac{g^2}{48\pi}} B_L^{ee} \right)^2 + 2 \sqrt{\frac{g^4 |V_{ud}|^2}{768\pi^2}} A_L^{ud} B_L^{ee} \geq \frac{g^2 V_{ud}}{8\sqrt{3}\pi} A_L^{ud} B_L^{ee}. \end{aligned} \quad (9)$$

The first inequality takes the equals sign at $A_L^{qq' \neq ud} = A_R^{qq'} = B_L^{\alpha\alpha \neq ee} = 0$, whereas the second inequality takes the equals sign at $\sqrt{g^2 |V_{ud}|^2 / 16\pi} A_L^{ud} = \sqrt{g^2 / 48\pi} B_L^{ee}$ ¹. These inequalities hold for all $A_{L,R}^{qq'}$ and $B_L^{\ell\ell}$ and set an upper bound on $\tilde{\epsilon}_{\alpha\alpha}^{qq'Y} \times M_{W'}^2$, when $\Gamma_{W'}/M_{W'}$ is fixed,

$$\left| \tilde{\epsilon}_{\alpha\alpha}^{qq'Y} \right| \leq \frac{8\sqrt{3}\pi M_{W'}^2}{g^2 |V_{qq'}| M_{W'}^2} \frac{\Gamma_{W'}}{M_{W'}}. \quad (10)$$

For simplicity, taking $|\tilde{\epsilon}_{ee}^{udY}|$ as an example, the maximally allowed $|\tilde{\epsilon}_{ee}^{udY}|$ as a function of $M_{W'}$ is shown in Fig. 2 for different values of the ratio $\Gamma_{W'}/M_{W'}$. The unitarity bounds given by Eq.(7) are also shown in Fig. 2. It can be seen that with additional assumptions on $\Gamma_{W'}/M_{W'}$, that is, for some values of $\Gamma_{W'}/M_{W'}$ and $M_{W'}$, tighter constraints can be obtained. For larger $M_{W'}$, the perturbative unitarity constraints become stronger than those from W' decays. If we take $\Gamma_{W'}/M_{W'} = 0.1$ [25, 26], $|\tilde{\epsilon}_{\alpha\alpha}^{qq'R}| \leq 10.868 \times M_W^2/M_{W'}^2$, for $1 \text{ TeV} \leq M_{W'} \leq 7 \text{ TeV}$, and $|\tilde{\epsilon}_{\alpha\alpha}^{qq'L}| \leq 10.868 \times M_W^2/M_{W'}^2$, for $M_{W'} \leq 4 \text{ TeV}$. Meanwhile, the perturbative unitarity constraints are $|\tilde{\epsilon}_{\alpha\alpha}^{qq'L}| \leq 7.584 \times M_W^2/M_{W'}^2$, $|\tilde{\epsilon}_{\alpha\alpha}^{qq'L}| \leq 3.637 \times M_W^2/M_{W'}^2$, and $|\tilde{\epsilon}_{\alpha\alpha}^{qq'L}| \leq 2.089 \times M_W^2/M_{W'}^2$, for $M_{W'} = 5 \text{ TeV}$, 6 TeV , and 7 TeV , respectively.

The theoretical constraints given in Fig. 2 are used as a reference for the MC studies in the next section. It can be seen from Fig. 2 that the larger the mass of the W' boson, the tighter the constraint on $|\tilde{\epsilon}_{ee}^{udL}|$. However, with fixed $\Gamma_{W'}/M_{W'}$, the W' contributions to the process $pp \rightarrow e^+ \nu_e$ typically decrease with increasing $M_{W'}$; therefore, the larger the value of

¹ The equal sign can be taken only in the sense of mathematics, which corresponds to the loosest case.

There is no physical motivation behind it. For a physical scenario this constraint should be even tighter.

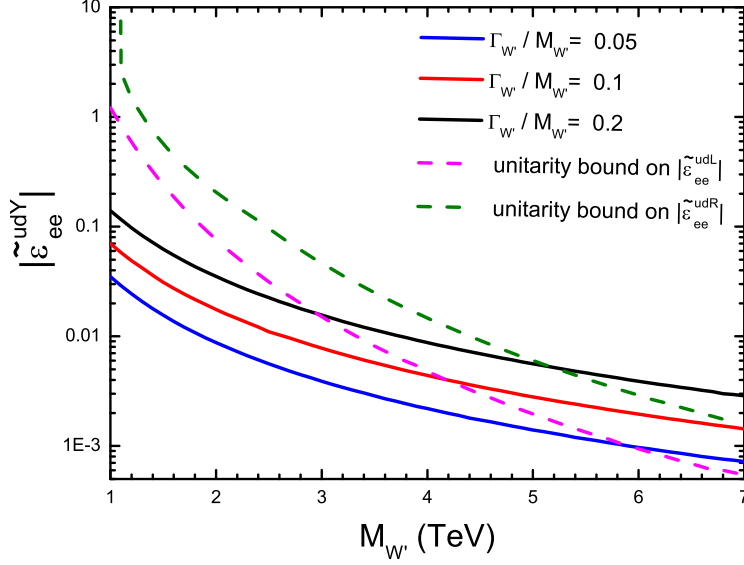


FIG. 2. Constraints on the CC NSI parameter $|\tilde{\epsilon}_{ee}^{udY}|$ from partial wave unitarity and W' decays for different values of the ratio $\Gamma_{W'}/M_{W'}$.

$M_{W'}$, the larger the value of $|\tilde{\epsilon}_{ee}^{udL}|$ needed to observe the signal at the LHC. However, $|\tilde{\epsilon}_{ee}^{udL}|$ must satisfy the unitarity constraint given by Eq. (7). In the following MC analysis, we take into account the theoretical constraints on the NSI parameters $|\tilde{\epsilon}_{\alpha\alpha}^{qq'Y}|$, set $\Gamma_{W'}/M_{W'} = 0.1$, and assume that the mass $M_{W'}$ is from 1 TeV to 7 TeV.

III. EXPECTED CONSTRAINTS ON $\tilde{\epsilon}_{\ell\ell}^{udY}$ AT THE LHC

A simple and efficient way to search for the gauge boson W' at the LHC is through its single s-channel resonance and subsequent leptonic decays [62]. Because the main components of protons are u and d quarks, the contribution of the $u\bar{d}$ process is considerably larger than that of the $c\bar{s}$ process. It has been noted that the luminosity of $u\bar{d}$ quarks is two orders of magnitude larger than that of $c\bar{s}$ quarks [63]. If $\tilde{\epsilon}_{\ell\ell}^{csY}$ are at the same magnitude as $\tilde{\epsilon}_{\ell\ell}^{udY}$, the contribution of $c\bar{s} \rightarrow \ell^+\nu_\ell$ is negligible compared with $u\bar{d} \rightarrow \ell^+\nu_\ell$; therefore, we neglect the contribution from non zero $\tilde{\epsilon}_{\ell\ell}^{qq'Y}$ with $qq' \neq ud$. In this paper, we consider the subprocess $u\bar{d} \rightarrow \ell^+\nu_\ell$ where ℓ is e or μ , which corresponds to $\tilde{\epsilon}_{ee}^{udY}$ or $\tilde{\epsilon}_{\mu\mu}^{udY}$. Fig. 3 shows the Feynman diagram of the subprocess $u\bar{d} \rightarrow \ell^+\nu_\ell$ ($\ell = e$ or μ) induced by W' exchange at the LHC.

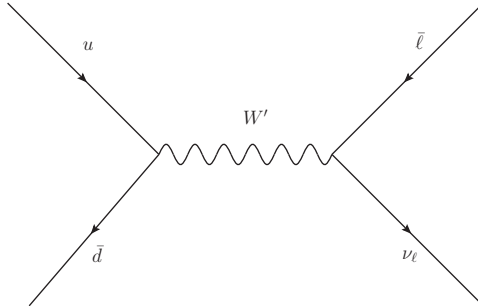


FIG. 3. Leading-order (LO) Feynman diagram for the single production of the W' boson and subsequent leptonic decays.

In numerical estimation, the Lagrangian described by Eq. (2) is implemented using FEYNRULES [64–66], and a Universal Feynrules Output (UFO) file is generated and taken into the MadGraph5_aMC@NLO toolkit [67, 68] with the standard cuts

$$p_T^\ell > 10 \text{ GeV}, |\eta_\ell| < 2.5.$$

A fast detector simulation is applied using Delphes [69] with the CMS detector card. The parton distribution functions are taken as NNPDF2.3 [70, 71]. To highlight the signal from the background, the kinematical features of the signal and background are studied using MadAnalysis5 [72]. The processes in the SM with the same final states are considered as the background. At tree level, there is only one type of background in which $\ell^+\nu_\ell$ are from the SM W boson. The main difference between the signal and the background is that for signal events, the leptons are from a W' boson with a considerably larger mass $M_{W'}$ than that of the SM W boson. As a consequence, the transverse momenta of charged leptons for signal events are generally larger than those for background events. p_T^ℓ has also been used in previous studies to highlight the signal of W' . The normalized distributions of p_T^ℓ for $pp \rightarrow e^+\nu_e$ are shown in Fig. 4. (a). It can be seen that p_T^ℓ is generally smaller than 360 GeV for background events, whereas the signal events have large p_T^ℓ tails. In this paper, we only keep events with $p_T^\ell \geq 360$ GeV. For the same reason, the missing transverse energy \cancel{E}_T for the signal events is also typically larger than those for the background events. The normalized distributions of \cancel{E}_T are shown in Fig. 4. (b). The background events are dominantly distributed in the region $\cancel{E}_T < 460$ GeV, which is not the case for the signal events. In this paper, we only keep events with $\cancel{E}_T \geq 460$ GeV. The normalized distributions for the process $pp \rightarrow \mu^+\nu_\mu$

are shown in Fig. 5. When searching for the signal of the W' boson with an unknown mass, the cuts are applied uniformly. However, the event selection strategies can be further improved. If the signal is not found, the goal should be to constrain the parameter $\tilde{\epsilon}$ for different $M_{W'}$. For this purpose, the event selection strategy can be different for different $M_{W'}$ and therefore, it can be further optimized according to $M_{W'}$. For $M_{W'} = 1$ TeV, which is close to the mass of the W boson in the SM, we use the looser cuts $p_T^\ell \geq 300$ GeV and $\cancel{E}_T \geq 250$ GeV.

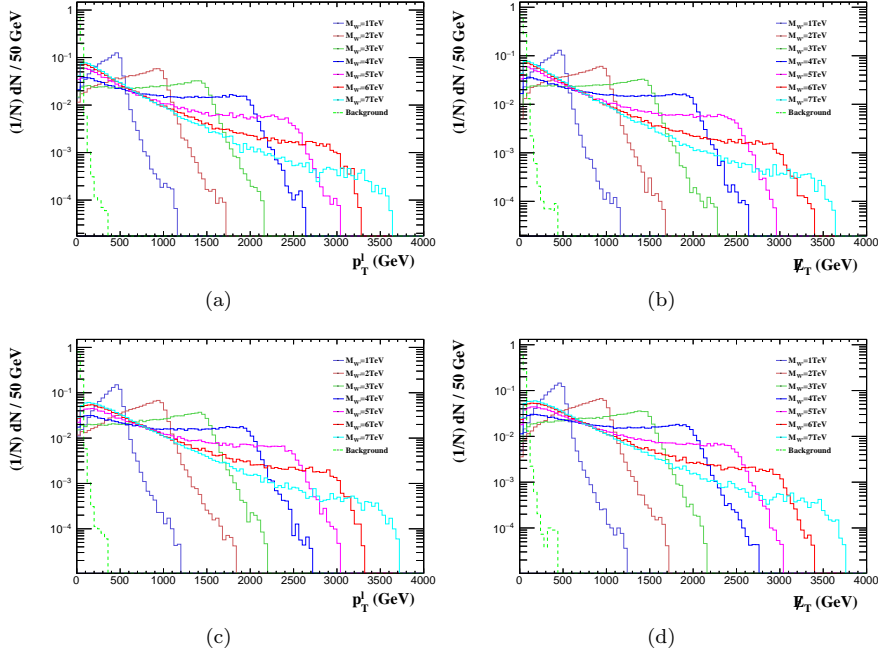


FIG. 4. For the process $pp \rightarrow e^+ \nu_e$, the normalized distributions of p_T^ℓ and \cancel{E}_T for the signal and background events. The cases for $A_R^{ud} = 0$ are shown in (a,b), while the cases for $A_L^{ud} = 0$ are shown in (c,d).

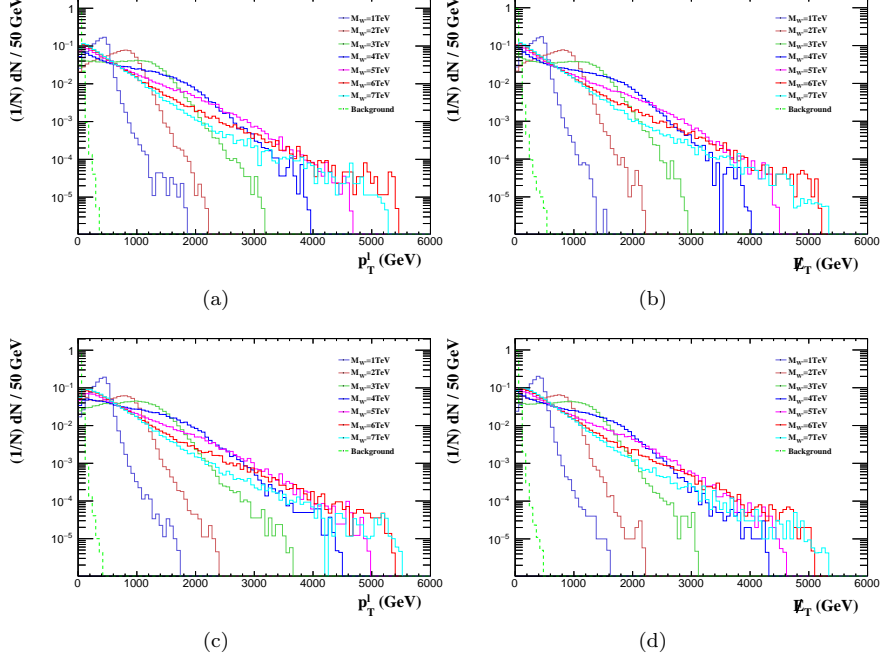


FIG. 5. Same as Fig. 4 but for the process $pp \rightarrow \mu^+ \nu_\mu$.

Because the masses of fermions are negligible, the interference between $\tilde{\epsilon}_{\ell\ell}^{qq'L}$ and $\tilde{\epsilon}_{\ell\ell}^{qq'R}$ is neglected in this study for simplicity. To focus on the sensitivities of the process on $\tilde{\epsilon}$, we assume $\tilde{\epsilon}$ is a real number in numerical estimations. The cross-sections of the process $pp \rightarrow \ell^+ \nu_\ell$ including the W' contributions can be parameterized as

$$\sigma^L(\tilde{\epsilon}) = \sigma_{SM} + \sigma_{INT}(\tilde{\epsilon}) + \sigma_{NSI}^L(\tilde{\epsilon}), \quad (11)$$

$$\sigma^R(\tilde{\epsilon}) = \sigma_{SM} + \sigma_{NSI}^R(\tilde{\epsilon}). \quad (12)$$

$\sigma_{INT}(\tilde{\epsilon}) = \alpha_{int} \times \tilde{\epsilon}$ originates from the interference between the SM and W' contribution, and σ_{NSI}^Y represents the contribution from only W' exchanges with $\sigma_{NSI}^Y(\tilde{\epsilon}) = \alpha_{nsi}^Y \times \tilde{\epsilon}^2$. After the event selection strategy, the dependencies of the factors α_{int} and α_{nsi}^Y on $M_{W'}$ can be fitted with the results of the MC simulation for different $M_{W'}$ at $\sqrt{s} = 13$ TeV, which are listed in Table I. For $M_{W'}^L = 2 \sim 7$ TeV, $\sigma_{SM}^{ee} = 0.0034$ pb and $\sigma_{SM}^{\mu\mu} = 0.0027$ pb ($\sigma_{SM}^{ee} = 0.021$ pb and $\sigma_{SM}^{\mu\mu} = 0.027$ pb for $M_{W'}^L = 1$ TeV owing to different event selection strategies). Taking $pp \rightarrow e^+ \nu_e$ as an example, the cross-sections of the process $pp \rightarrow e^+ \nu_e$ after cuts for different $M_{W'}$ are shown in Fig. 6. The numerical results fit the bilinear functions in Eqs. (11) and (12) very well. Fig. 6 shows that the interference plays an important role in $\sigma^L(\tilde{\epsilon})$. Moreover, as shown Fig. 6 and presented in the next section, the sensitivity of the

process $pp \rightarrow \ell^+ \nu_\ell$ on W' at the LHC has already reached the region where the interference effect should be considered.

TABLE I. After the event selection strategy, α_{int} and α_{nsi}^Y are fitted for different $M_{W'}$ at $\sqrt{s} = 13$ TeV.

$M_{W'}$ (TeV)	$pp \rightarrow e^+ \nu_e$			$pp \rightarrow \mu^+ \nu_\mu$		
	α_{int} (pb)	α_{nsi}^L (pb)	α_{nsi}^R (pb)	α_{int} (pb)	α_{nsi}^L (pb)	α_{nsi}^R (pb)
1	-3.29	6873.86	8878.72	-3.18	9127.30	8360.4
2	-2.49	5215.94	5911.49	-2.31	5966.57	5872.99
3	-2.45	3225.12	3164.77	-2.43	3618.67	3518.60
4	-2.23	1621.66	1584.89	-2.14	1754.81	1668.15
5	-2.07	964.73	893.93	-2.07	1030.03	881.07
6	-2.07	649.12	614.93	-1.88	669.24	604.85
7	-1.95	508.87	501.16	-1.84	511.24	499.81

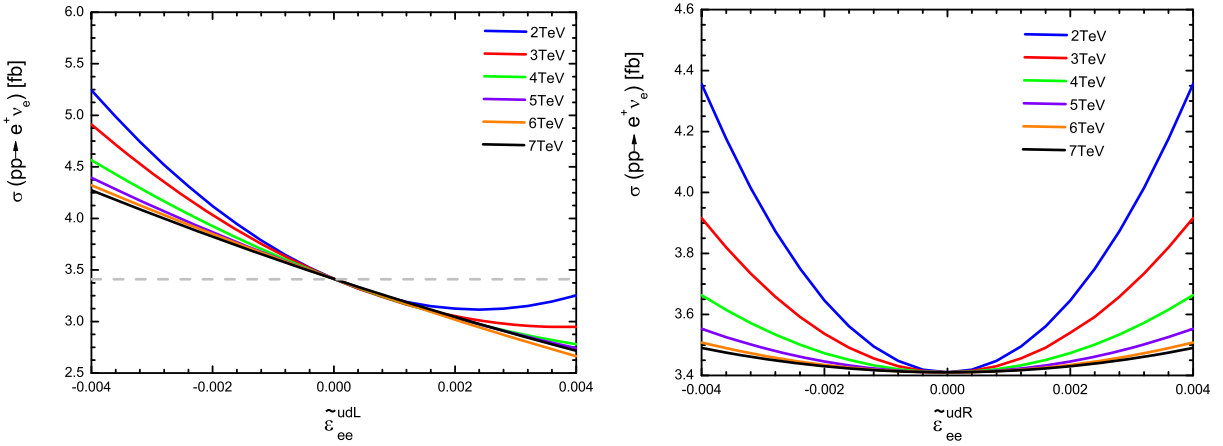


FIG. 6. After the event selection strategy, the relationship between $\tilde{\epsilon}_{ee}^{udL}$ (left panel), $\tilde{\epsilon}_{ee}^{udR}$ (right panel), and the cross-section of the process $pp \rightarrow e^+ \nu_e$ for different $M_{W'}$. The case of $M_{W'} = 1$ TeV is not shown.

The expected constraints on $\tilde{\epsilon}$ are estimated with the help of the statistical significance defined as

$$\mathcal{S}_{stat} = \sqrt{\mathcal{L}} \times \left(\left| \sigma \left(\tilde{\epsilon}_{\ell\ell}^{qq'Y} \right) - \sigma_{SM} \right| / \sqrt{\sigma \left(\tilde{\epsilon}_{\ell\ell}^{qq'Y} \right)} \right), \quad (13)$$

where σ_{SM} and $\sigma\left(\tilde{\epsilon}_{\ell\ell}^{qq'Y}\right)$ are the SM cross-section and total cross-section including the W' contributions after cuts are applied, respectively. When $\tilde{\epsilon}_{\ell\ell}^{qq'L}$ and $\tilde{\epsilon}_{\ell\ell}^{qq'R}$ are both non zero, $\sigma(\tilde{\epsilon}^L, \tilde{\epsilon}^R) = \sigma_{SM} + \sigma_{INT}(\tilde{\epsilon}^L) + \sigma_{NSI}^L(\tilde{\epsilon}^L) + \sigma_{NSI}^R(\tilde{\epsilon}^R)$. For $\mathcal{S}_{stat} = 2, 3,$ and 5 , the upper limits on the $\tilde{\epsilon}_{ee}^{udL}$ and $\tilde{\epsilon}_{ee}^{udR}$ plane are shown in Fig. 7. For clarity, in Fig. 7, we use the signal significance of events that exceed the SM. The constraints are approximate eccentric ellipses, indicating the importance of the interference term.

TABLE II. Expected constraints on $\tilde{\epsilon}_{\ell\ell}^{udY}$ detected at the $2\sigma, 3\sigma,$ and 5σ confidence levels (CLs).

	$\tilde{\epsilon}_{ee}^{udL}(\times 10^{-4})$	$\tilde{\epsilon}_{ee}^{udR}(\times 10^{-4})$	$\tilde{\epsilon}_{\mu\mu}^{udL}(\times 10^{-4})$	$\tilde{\epsilon}_{\mu\mu}^{udR}(\times 10^{-4})$
2σ	$[-1.78, 3.36]$	$[-8.09, 8.09]$	$[-1.77, 3.35]$	$[-7.31, 7.31]$
3σ	$[-2.45, 4.10]$	$[-10.02, 10.02]$	$[-2.43, 4.09]$	$[-9.55, 9.55]$
5σ	$[-4.08, 5.24]$	$[-13.23, 13.23]$	$[-3.92, 5.20]$	$[-12.61, 12.61]$

To study the sensitivities, it is assumed that only one of $\tilde{\epsilon}_{\ell\ell}^{qq'L}$ and $\tilde{\epsilon}_{\ell\ell}^{qq'R}$ is non zero. For $M_{W'}$ in the range of $1 \text{ TeV} \sim 7 \text{ TeV}$, the expected constraints on $\tilde{\epsilon}_{\ell\ell}^{udY}$ at the $2\sigma, 3\sigma,$ and 5σ confidence levels (CLs) are shown in Table II. In Figs. 8 and 9, we show the expected constraints on $\tilde{\epsilon}_{ee}^{udL(R)}$ and $\tilde{\epsilon}_{\mu\mu}^{udL(R)}$ for different $M_{W'}$ at the 13 TeV LHC with $\mathcal{L} = 139 \text{ fb}^{-1}$. The tightest theoretical constraints discussed in Sec. II are also presented in Figs. 8 and 9. The results of $\tilde{\epsilon}_{\ell\ell}^{udY}$ satisfy the unitarity bounds generated by Eq. (7) and satisfy the constraints given by Eq. (10). From Figs. 8 and 9, we find that for different $M_{W'}$, the expected constraints are similar for $\tilde{\epsilon}_{\ell\ell}^{udL}$. This can be understood by looking at Table I; α_{int} are at the same order of magnitude. Therefore, when the interference term is dominant, the expected constraints are insensitive to $M_{W'}$. For the same reason, the positive and negative expected constraints are different for $\tilde{\epsilon}_{\ell\ell}^{udL}$. This is not the case for $\tilde{\epsilon}_{\ell\ell}^{udR}$. Because there is no interference, the expected constraints on $\tilde{\epsilon}_{\ell\ell}^{udR}$ are generally looser than those on $\tilde{\epsilon}_{\ell\ell}^{udL}$. Except for the case of $M_{W'} = 1 \text{ TeV}$, the expected constraints are looser when $M_{W'}$ is larger because the cross-section decreases rapidly with increasing $M_{W'}$. For $M_{W'} = 1 \text{ TeV}$, the mass of the W' boson is closer to that of the SM W boson; therefore, the event selection strategy is less efficient. As a consequence, even though the cross-section of the signal is larger, a stronger expected constraint cannot be reached compared with the case of $M_{W'} = 2 \text{ TeV}$.

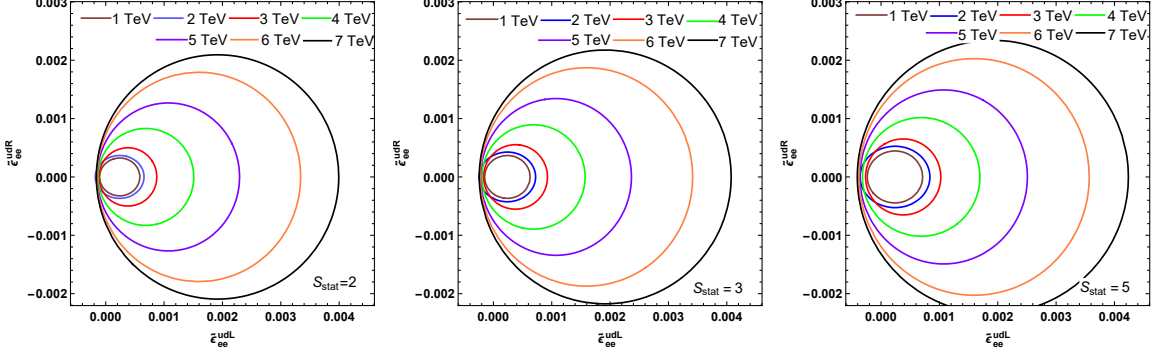


FIG. 7. For \mathcal{S}_{stat} equaling 2 (left panel), 3 (middle panel), and 5 (right panel), the relationship between the expected constraints on $\tilde{\epsilon}_{ee}^{udL}$ and $\tilde{\epsilon}_{ee}^{udR}$ at the 13 TeV LHC with $\mathcal{L} = 139 \text{ fb}^{-1}$.

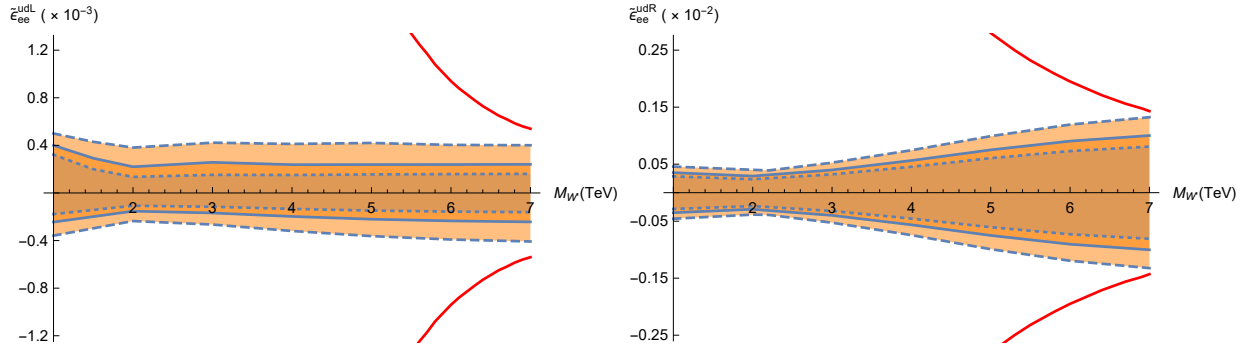


FIG. 8. For \mathcal{S}_{stat} equaling 2 (dotted line), 3 (solid line), and 5 (dashed line), the expected constraints on $\tilde{\epsilon}_{ee}^{udL}$ (left panel) and $\tilde{\epsilon}_{ee}^{udR}$ (right panel) as functions of $M_{W'}$ at the 13 TeV LHC with $\mathcal{L} = 139 \text{ fb}^{-1}$. The red solid lines originate from the tightest theoretical constraints.

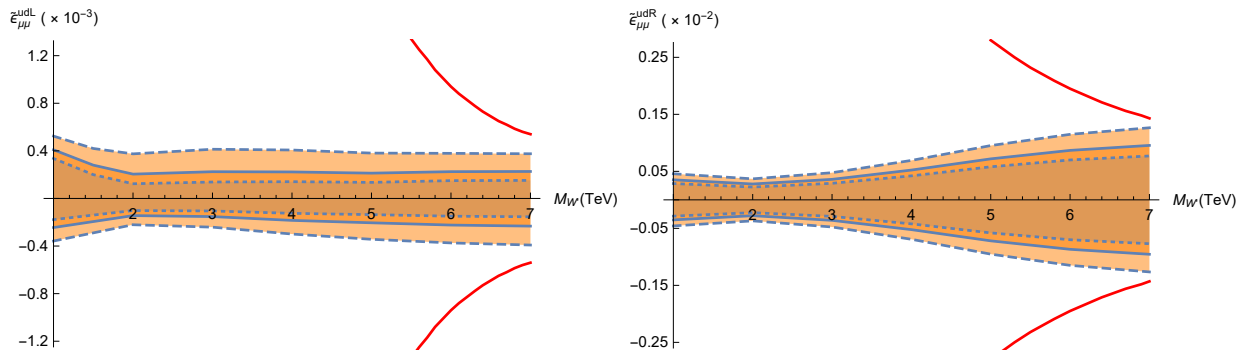


FIG. 9. Same as Fig. 8 but for $\tilde{\epsilon}_{\mu\mu}^{udL}$ (left panel) and $\tilde{\epsilon}_{\mu\mu}^{udR}$ (right panel).

It is interesting to discuss the expected constraints for special cases. In the case of $|A_Y^{qq'}| = |B_L^{\alpha\alpha}| = 1$, which corresponds to the SSM [73], the expected constraints on $\tilde{\epsilon}$ can be

translated to the lower bounds on $M_{W'}$. The results are shown in Fig. 10. However, because the MC simulation is carried out for fixed $M_{W'}$, if the lower bound on $M_{W'}$ is larger than the value of $M_{W'}$ used in the simulation, such value should be ruled out. Consequently, an expected constraint can be set on $M_{W'}$. The expected constraints of the process $pp \rightarrow e^+\nu_e$ on $M_{W'}$ for $\mathcal{S}_{stat} = 2, 3,$ and 5 are $M_{W'} > 6.3$ TeV, $M_{W'} > 5.2$ TeV, and $M_{W'} > 3.8$ TeV, respectively. The expected constraints of the process $pp \rightarrow \mu^+\nu_\mu$ on $M_{W'}$ for $\mathcal{S}_{stat} = 2, 3,$ and 5 are $M_{W'} > 6.5$ TeV, $M_{W'} > 5.4$ TeV, and $M_{W'} > 3.9$ TeV, respectively. The results of the LHC experiments are $M_{W'} > 6.0$ TeV for the $e\nu_e$ channel and $M_{W'} > 5.0$ TeV for the $\mu\nu_\mu$ channel at the 2σ CL (we choose the largest lower bounds from Refs. [36–39]). By considering the interference effect, these results can be further improved.

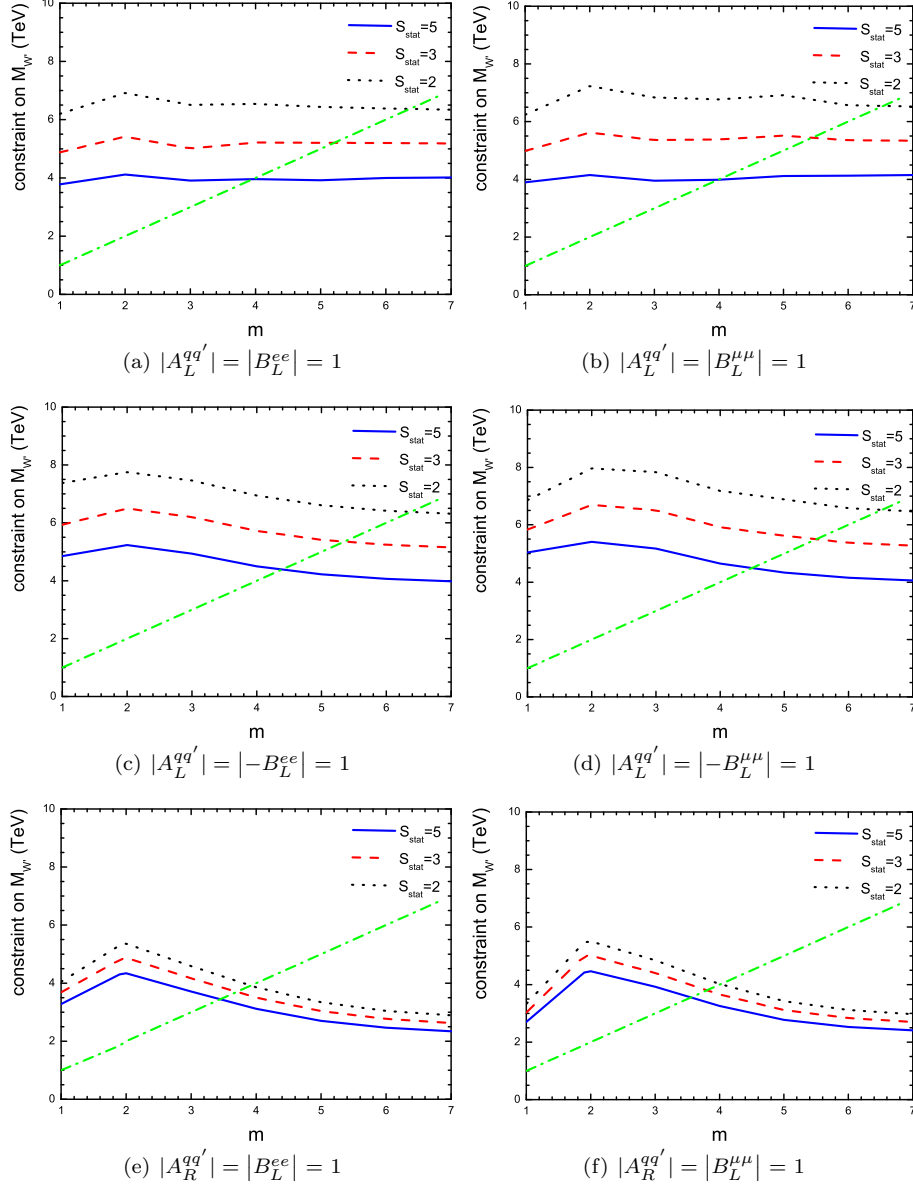


FIG. 10. For $|A_Y^{qq'}| = |B_L^{\alpha\alpha}| = 1$, the expected constraints on $M_{W'}$ obtained by events generated at $M_{W'} = m$. $M_{W'}$ on the left hand side of the dashed-dotted line is ruled out. The intersection of the dashed-dotted lines and the dotted lines gives the lower bound for $\mathcal{S}_{stat} = 2$ as an example.

IV. SENSITIVITIES OF THE HL-LHC TO $\tilde{\epsilon}_{\ell\ell}^{udY}$

In this section, sensitivities to $\tilde{\epsilon}_{\ell\ell}^{udY}$ in future runs of the LHC with higher luminosity, known as the HL-LHC, are investigated. We assume that the HL-LHC runs at $\sqrt{s} = 14$ TeV with integrated luminosities of 300 fb^{-1} , 1 ab^{-1} , and 3 ab^{-1} [74, 75]. Taking the

process $pp \rightarrow e^+\nu_e$ as an example, the normalized distributions of p_T^ℓ and \cancel{E}_T for the signal and background are shown in Fig. 11.

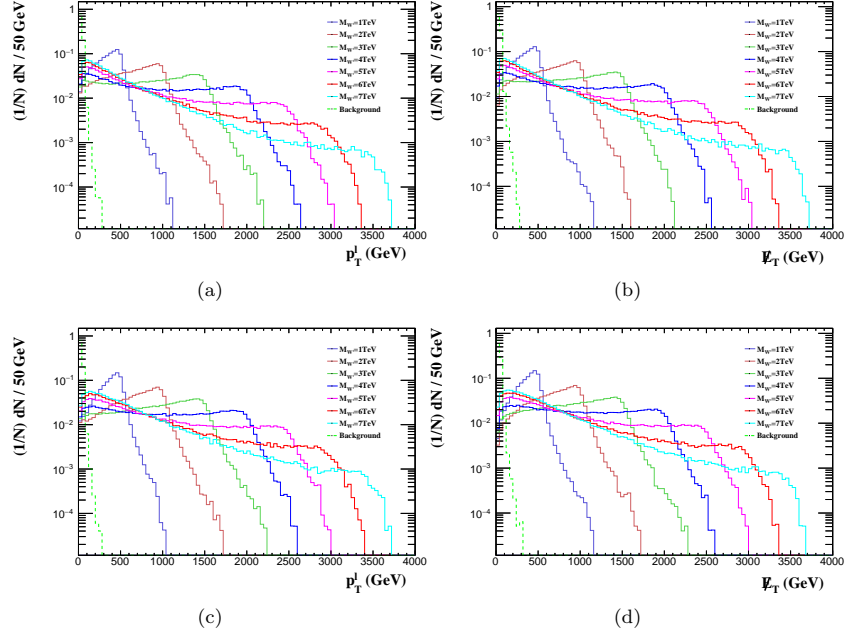


FIG. 11. Same as Fig. 4 but for the HL-LHC at $\sqrt{s} = 14$ TeV with $\mathcal{L} = 300 \text{ fb}^{-1}$.

According to Fig. 11, for different masses (1 TeV \sim 7 TeV), we choose the same cuts such that $p_T^\ell \geq 300$ GeV and $\cancel{E}_T \geq 280$ GeV for $pp \rightarrow e^+\nu_e$ and $p_T^\ell \geq 300$ GeV and $\cancel{E}_T \geq 340$ GeV for $pp \rightarrow \mu^+\nu_\mu$. The cross-sections after cuts are also fitted using Eqs. (11) and (12), $\sigma_{SM}^{ee} = 0.022$ pb, and $\sigma_{SM}^{\mu\mu} = 0.016$ pb. The results are shown in Table III and Fig. 12. The upper limits on the $\tilde{\epsilon}_{ee}^{udL}$ and $\tilde{\epsilon}_{ee}^{udR}$ plane at the 14 TeV LHC with $\mathcal{L} = 300 \text{ fb}^{-1}$ are shown in Fig. 13.

TABLE III. Same as Table I but for the HL-LHC with $\sqrt{s} = 14$ TeV.

$M_{W'}$ (TeV)	$pp \rightarrow e^+\nu_e$			$pp \rightarrow \mu^+\nu_\mu$		
	α_{int} (pb)	α_{nsi}^L (pb)	α_{nsi}^R (pb)	α_{int} (pb)	α_{nsi}^L (pb)	α_{nsi}^R (pb)
1	-6.98	7782.23	6169.75	-7.01	7171.98	6588.00
2	-7.47	8729.47	6650.92	-7.18	8159.10	8507.71
3	-6.86	4910.34	4990.20	-6.76	4752.89	5137.76
4	-6.54	2510.25	2514.10	-6.06	2993.21	2888.60
5	-6.16	1256.88	1522.74	-5.68	1227.32	1638.96
6	-5.89	1146.44	1145.43	-5.67	1357.43	1120.93
7	-5.38	1067.50	798.57	-5.46	680.62	1054.37

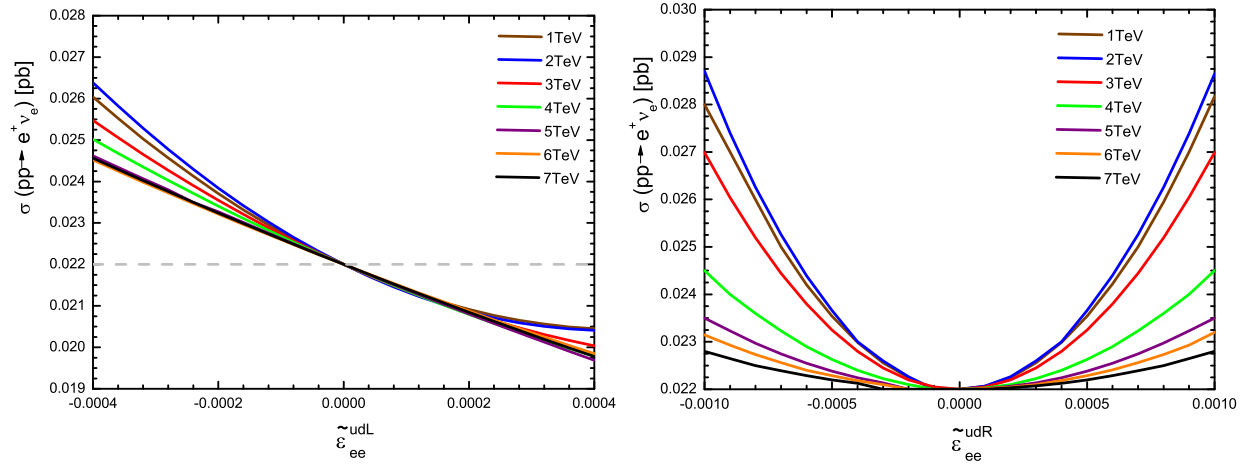


FIG. 12. Same as Fig. 6 but for the HL-LHC with $\sqrt{s} = 14$ TeV.

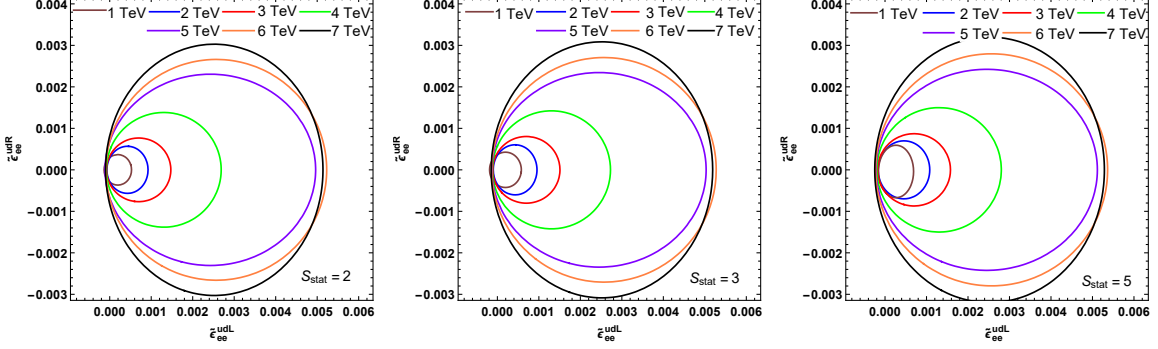


FIG. 13. Same as Fig. 7 but for the HL-LHC with $\sqrt{s} = 14$ TeV.

The sensitivities of the process $pp \rightarrow l^+ \nu_l$ at the 14 TeV LHC with $\mathcal{L} = 300 \text{ fb}^{-1}$ to $\tilde{\epsilon}_{\ell\ell}^{udY}$ are estimated with the help of \mathcal{S}_{stat} . The numerical results are summarized in Figs. 14 and 15.

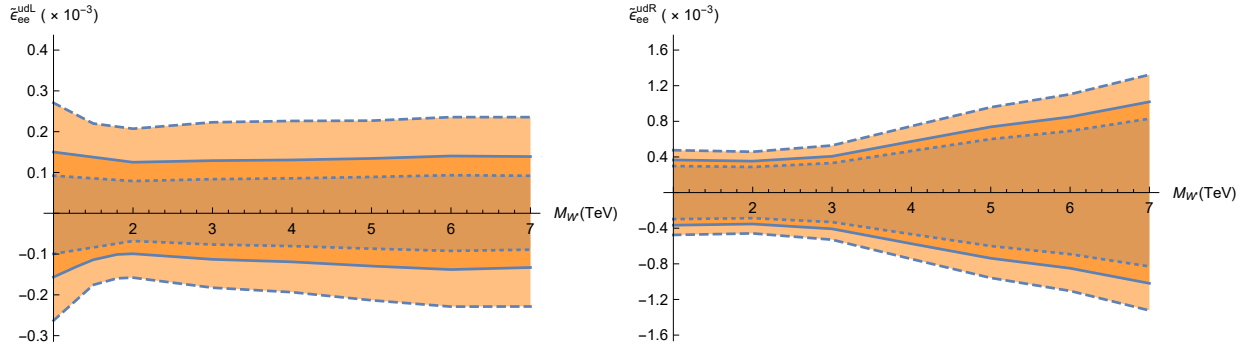


FIG. 14. Same as Fig. 8 but for $\tilde{\epsilon}_{ee}^{udL}$ (left panel) and $\tilde{\epsilon}_{ee}^{udR}$ (right panel) at the 14 TeV HL-LHC with $\mathcal{L} = 300 \text{ fb}^{-1}$.

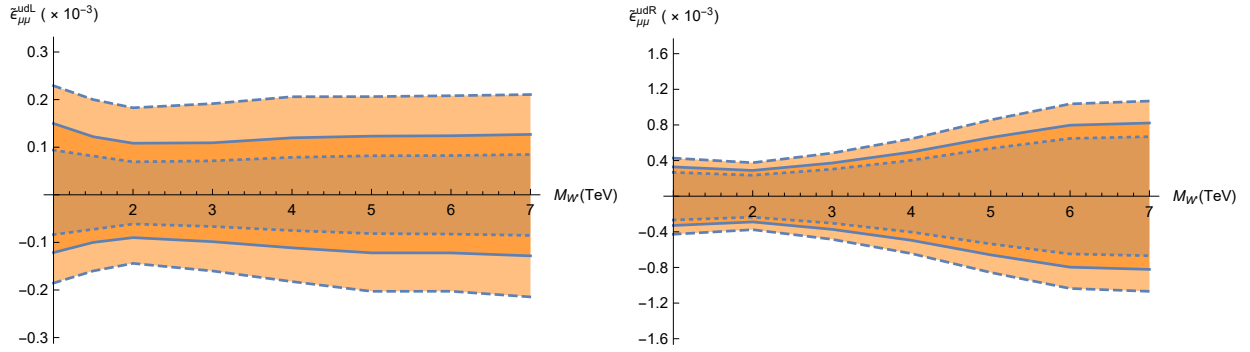


FIG. 15. Same as Fig. 14 but for $\tilde{\epsilon}_{\mu\mu}^{udL}$ (left panel) and $\tilde{\epsilon}_{\mu\mu}^{udR}$ (right panel).

As shown in Figs. 14 and 15, $\tilde{\epsilon}_{\ell\ell}^{udY}$ satisfies the unitarity bounds generated by Eq. (7) and is

also within the constraints given by Eq. (10). Comparing these figures with Figs. 8 and 9, the HL-LHC is more sensitive to the W' boson than the LHC. The results for higher luminosities, $\mathcal{L} = 1 \text{ ab}^{-1}$ and 3 ab^{-1} , are also investigated and shown in Fig. 16. Compared with those at the 13 TeV LHC with $\mathcal{L} = 139 \text{ fb}^{-1}$, the expected constraints can be strengthened to approximately an order of magnitude for the 14 TeV LHC with $\mathcal{L} = 3 \text{ ab}^{-1}$.

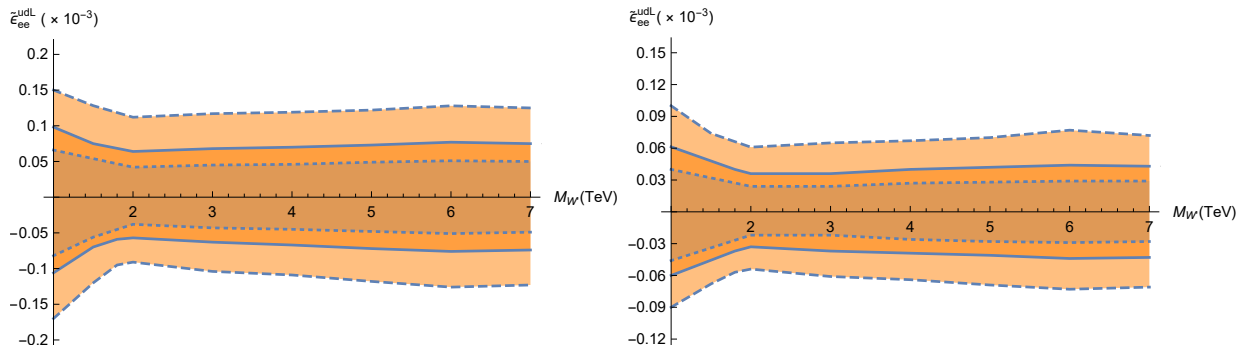


FIG. 16. Same as Fig. 14 but for $\tilde{\epsilon}_{ee}^{udL}$ at the 14 TeV LHC with $\mathcal{L} = 1 \text{ ab}^{-1}$ (left panel) and 3 ab^{-1} (right panel).

V. CONCLUSIONS AND DISCUSSIONS

Many extensions of the SM predict the presence of charged heavy gauge bosons that might be found at the LHC, which are commonly referred to as the W' boson and can induce the CC NSI. In this paper, the contributions of W' bosons to the process $pp \rightarrow \ell\nu$ are investigated. Before MC simulation, we first consider the theoretical constraints on the simplified W' model and further on $\tilde{\epsilon}_{\ell\ell}^{qq'Y}$ from two perspectives: the partial wave unitarity and W' decays. Our numerical calculation shows that interference effects play a vital role, and as a consequence, the expected constraints on $\tilde{\epsilon}^L$ are not less mass-dependent than in previous studies. The event selection strategy is then studied. With the help of \mathcal{S}_{stat} , the expected constraints on $\tilde{\epsilon}$ are estimated. For the integrated luminosities considered in this paper, the expected constraints are insensitive to the nature of neutrinos (Dirac or Majorana) [76].

To date, there have been many studies on the constraints on NC NSI. For example, Ref. [26] proposed that the LHC sensitivity to NC NSIs is $\tilde{\epsilon} \leq 2 \times 10^{-3}$ for $M_{Z'} = 2 \text{ TeV}$, and the result of Ref. [25] shows that in the simplified Z' model, the upper limits on $\tilde{\epsilon}$ are

0.042 and 0.0028 corresponding to Z' with $M_{Z'} = 0.2$ and 2 TeV, respectively. However, up to our knowledge, studies on the new gauge boson W' mainly focus on the constraints on its mass and couplings, and there are few studies on the CC NSI in the context of a simplified W' model, especially at the current and future LHC. We focus on the expected constraints of collider experiments on the CC NSI induced by W' . The expected constraints on the CC NSI parameters at the 2σ CL are $-1.78 \times 10^{-4} \leq \tilde{\epsilon}_{ee}^{udL} \leq 3.36 \times 10^{-4}$ and $-1.77 \times 10^{-4} \leq \tilde{\epsilon}_{\mu\mu}^{udL} \leq 3.35 \times 10^{-4}$ at the 13 TeV LHC with $\mathcal{L} = 139 \text{ fb}^{-1}$. Ref. [77] carefully analyzed the contributions of W' to several low-energy observables, such as the leptonic decays of charged pion mesons, semileptonic τ decay, lepton flavor universality in pion mesons, CKM unitarity, and superallowed β decays. Among them, the tightest constraints are $\epsilon_{ee}^{udV} = 7.10 \times 10^{-4}$ from superallowed β decays and $\epsilon_{ee}^{udA} = -1.85 \times 10^{-2}$ from the decay $\pi^+ \rightarrow e^+ \nu_e$, which result in $|\epsilon_{ee}^{udL}| < 8.895 \times 10^{-3}$ and $|\epsilon_{ee}^{udR}| < 9.61 \times 10^{-3}$. Thus, the expected constraints on the CC NSI parameters at the LHC are approximately an order of magnitude tighter than those from low-energy observables. ATLAS and CMS presented the analysis of data with $L = 36 \text{ fb}^{-1}$ at $\sqrt{s} = 13 \text{ TeV}$, setting the constraints as $M_{W'} > 5.2 \text{ TeV}$ in the electron channel [36] and $M_{W'} > 4.9 \text{ TeV}$ in the muon channel [38], at the 2σ CL using the SSM, which is looser than the constraints 6.3 TeV and 6.5 TeV in our paper. Moreover, the expected constraints at the 14 TeV LHC with $\mathcal{L} = 3 \text{ ab}^{-1}$ can further narrow down the expected constraints to one order of magnitude from those at the 13 TeV LHC. We propose that the interference effects are non-negligible and should be considered in future studies.

ACKNOWLEDGMENT

This work was partially supported by the National Natural Science Foundation of China under Grant Nos. 11875157 and 12147214, the Natural Science Foundation of the Liaoning Scientific Committee No. LJKZ0978 and the Outstanding Research Cultivation Program of Liaoning Normal University (No. 21GDL004).

[1] V. Barger, D. Marfatia, and K. Whisnant, Progress in the physics of massive neutrinos, *Int. J. Mod. Phys. E* **12**, 569 (2003).

- [2] M. C. Gonzalez-Garcia and M. Maltoni, Phenomenology with Massive Neutrinos, [Phys. Rept. **460**, 1 \(2008\)](#).
- [3] L. Wolfenstein, Neutrino Oscillations in Matter, [Phys. Rev. D **17**, 2369 \(1978\)](#).
- [4] D. Choudhury, K. Ghosh, and S. Niyogi, Probing nonstandard neutrino interactions at the LHC Run II, [Phys. Lett. B **784**, 248 \(2018\)](#).
- [5] T. Ohlsson, Status of non-standard neutrino interactions, [Rep. Prog. Phys. **76**, 044201 \(2013\)](#).
- [6] O. G. Miranda and H. Nunokawa, Non standard neutrino interactions: current status and future prospects, [New J. Phys. **17**, 095002 \(2015\)](#).
- [7] Y. Farzan and M. Tortola, Neutrino Oscillations and Non-Standard Interactions, [Front. in Phys. **6**, 10 \(2018\)](#).
- [8] I. Esteban, M. C. Gonzalez-Garcia, M. Maltoni, I. Martinez-Soler, and J. Salvado, Updated constraints on non-standard interactions from global analysis of oscillation data, [JHEP **08**, 180 \(2018\)](#) [Addendum: [JHEP **12**, 152 \(2020\)](#)].
- [9] M. C. Gonzalez-Garcia, M. Maltoni, and J. Salvado, Testing matter effects in propagation of atmospheric and long-baseline neutrinos, [JHEP **05**, 075 \(2011\)](#).
- [10] M. C. Gonzalez-Garcia and M. Maltoni, Determination of matter potential from global analysis of neutrino oscillation data, [JHEP **09**, 152 \(2013\)](#).
- [11] S. Davidson and V. Sanz, Non-Standard Neutrino Interactions at Colliders, [Phys. Rev. D **84**, 113011 \(2011\)](#).
- [12] A. Friedland, M. L. Graesser, I. M. Shoemaker, and L. Vecchi, Probing Nonstandard Standard Model Backgrounds with LHC Monojets, [Phys. Lett. B **714**, 267 \(2012\)](#).
- [13] D. Buarque Franzosi, M. T. Frandsen, and I. M. Shoemaker, New or ν missing energy: Discriminating dark matter from neutrino interactions at the LHC, [Phys. Rev. D **93**, 095001 \(2016\)](#).
- [14] K. S. Babu, P. S. B. Dev, S. Jana, and A. Thapa, Non-Standard Interactions in Radiative Neutrino Mass Models, [JHEP **03**, 006 \(2020\)](#).
- [15] J. Terol-Calvo, M. Tórtola, and A. Vicente, High-energy constraints from low-energy neutrino nonstandard interactions, [Phys. Rev. D **101**, 095010 \(2020\)](#).
- [16] F. J. Escrivuela, M. Tortola, J. W. F. Valle, and O. G. Miranda, Global constraints on muon-neutrino non-standard interactions, [Phys. Rev. D **83**, 093002 \(2011\)](#).

- [17] W. Altmannshofer, M. Tamaro, and J. Zupan, Non-standard neutrino interactions and low energy experiments, [JHEP **09**, 083 \(2009\)](#).
- [18] C. X. Yue, X. J. Cheng, Y. Q. Wang, and Y. Y. Li, Searching for the charged-current non-standard neutrino interactions at the e^-p colliders, [Nucl. Phys. B **982**, 115894 \(2022\)](#).
- [19] S. Davidson, C. Pena-Garay, N. Rius, and A. Santamaria, Present and future bounds on non-standard neutrino interactions, [JHEP **03**, 011 \(2003\)](#).
- [20] C. Biggio, M. Blennow, and E. Fernández-Martínez, General bounds on non-standard neutrino interactions, [JHEP **08**, 090 \(2009\)](#).
- [21] O. Cheung, C. J. Ouseph, and T. Wang, Non-standard neutrino and Z' interactions at the $\text{FASER}\nu$ and the LHC, [JHEP **12**, 209 \(2019\)](#).
- [22] I. Bischer, W. Rodejohann, and X. J. Xu, Loop-induced Neutrino Non-Standard Interactions, [JHEP **10**, 096 \(2018\)](#).
- [23] P. Coloma, M. C. Gonzalez-Garcia, and M. Maltoni, Loop-induced Neutrino Non-Standard Interactions, [JHEP **01**, 114 \(2021\)](#).
- [24] S. Pandey, S. Karmakar, and S. Rakshit, Strong constraints on non-standard neutrino interactions: LHC vs. IceCube, [JHEP **11**, 046 \(2019\)](#).
- [25] D. Liu, C. Sun, and J. Gao, Constraints on neutrino non-standard interactions from LHC data with large missing transverse momentum, [JHEP **02**, 033 \(2021\)](#).
- [26] K. S. Babu, D. Gonçalves, S. Jana, and P. A. N. Machado, Neutrino Non-Standard Interactions: Complementarity Between LHC and Oscillation Experiments, [Phys. Lett. B **815**, 136131 \(2021\)](#).
- [27] R. N. Mohapatra and J. C. Pati, Left-right gauge symmetry and an isoconjugate model of CP violation, [Phys. Rev. D **11**, 566 \(1975\)](#).
- [28] G. Senjanovic and R. N. Mohapatra, Exact Left-Right Symmetry and Spontaneous Violation of Parity, [Phys. Rev. D **12**, 1502 \(1975\)](#).
- [29] N. Arkani-Hamed, A. G. Cohen, E. Katz, and A. E. Nelson, The Littlest Higgs, [JHEP **07**, 034 \(2002\)](#).
- [30] T. Appelquist, H. C. Cheng, and B. A. Dobrescu, Bounds on universal extra dimensions, [Phys. Rev. D **64**, 035002 \(2001\)](#).
- [31] K. Agashe, S. Gopalakrishna, T. Han, G. Y. Huang, and A. Soni, LHC Signals for Warped Electroweak Charged Gauge Bosons, [Phys. Rev. D **80**, 075007 \(2009\)](#).

- [32] G. Aad *et al.* (ATLAS), ATLAS search for a heavy gauge boson decaying to a charged lepton and a neutrino in pp collisions at $\sqrt{s} = 7$ TeV, [Eur. Phys. J. C **72**, 2241 \(2012\)](#).
- [33] S. Chatrchyan *et al.* (CMS), Search for leptonic decays of W' bosons in pp collisions at $\sqrt{s} = 7$ TeV, [JHEP **08**, 023 \(2012\)](#).
- [34] G. Aad *et al.* (ATLAS), Search for new particles in events with one lepton and missing transverse momentum in pp collisions at $\sqrt{s} = 8$ TeV with the ATLAS detector, [JHEP **09**, 037 \(2014\)](#).
- [35] V. Khachatryan *et al.* (CMS), Search for physics beyond the standard model in final states with a lepton and missing transverse energy in proton-proton collisions at $\sqrt{s} = 8$ TeV, [Phys. Rev. D **91**, 092005 \(2015\)](#).
- [36] M. Aaboud *et al.* (ATLAS), Search for a new heavy gauge boson resonance decaying into a lepton and missing transverse momentum in 36 fb^{-1} of pp collisions at $\sqrt{s} = 13$ TeV with the ATLAS experiment, [Eur. Phys. J. C **78**, 401 \(2018\)](#).
- [37] V. Khachatryan *et al.* (CMS), Search for heavy gauge W' boson in events with an energetic lepton and large missing transverse momentum at $\sqrt{s} = 13$ TeV, [Phys. Lett. B **770**, 278 \(2017\)](#).
- [38] A. M. Sirunyan *et al.* (CMS), Search for high-mass resonances in final states with a lepton and missing transverse momentum at $\sqrt{s} = 13$ TeV, [JHEP **06**, 128 \(2018\)](#).
- [39] G. Aad *et al.* (ATLAS), Search for a heavy charged boson in events with a charged lepton and missing transverse momentum from pp collisions at $\sqrt{s} = 13$ TeV with the ATLAS detector, [Phys. Rev. D **100**, 052013 \(2019\)](#).
- [40] P. Osland, A. A. Pankov, and I. A. Serenkova, Updated constraints on Z' and W' bosons decaying into bosonic and leptonic final states using the run 2 ATLAS data, [Phys. Rev. D **103**, 053009 \(2021\)](#).
- [41] J. Fiaschi, F. Giuli, F. Hautmann, and S. Moretti, Enhancing the Large Hadron Collider sensitivity to charged and neutral broad resonances of new gauge sectors, [JHEP **02**, 179 \(2022\)](#).
- [42] R. Calabrese, A. D. Iorio, D. F. G. Fiorillo, A. O. M. Iorio, S. Morisi, and G. Miele, Top-flavor scheme in the context of W' searches at LHC, [Phys. Rev. D **104**, 055006 \(2021\)](#).
- [43] P. Coloma, I. Esteban, M. C. Gonzalez-Garcia, and M. Maltoni, Improved global fit to Non-Standard neutrino Interactions using COHERENT energy and timing data, [JHEP **02**, 023](#)

- (2020), [Addendum: JHEP 12, 071 (2020)].
- [44] P. S. B. Dev, K. S. Babu, P. B. Denton, Neutrino Non-Standard Interactions: A Status Report, *SciPost Phys.Proc.* **02**, 001 (2019).
 - [45] C. Biggio, M. Blennow, and E. Fernández-Martínez, Loop bounds on non-standard neutrino interactions, *JHEP* **03**, 139 (2009).
 - [46] C. Soumya, M. Ghosh, S. K. Raut, N. Sinha, and P. Mehta, Probing muonic charged current nonstandard interactions at decay-at-rest facilities in conjunction with T2HK, *Phys. Rev. D* **101**, 055009 (2020).
 - [47] A. D. Santos, Sensitivity of reactor experiments to nonstandard neutrino interactions in beta decay rates (2020), [arXiv:2007.07409](https://arxiv.org/abs/2007.07409).
 - [48] Z. Sullivan, Fully Differential W' Production and Decay at Next-to-Leading Order in QCD, *Phys. Rev. D* **66**, 075011 (2002).
 - [49] S. Gopalakrishna, T. Han, I. Lewis, Z. G. Si, and Y. F. Zhou, Chiral Couplings of W' and Top Quark Polarization at the LHC, *Phys. Rev. D* **82**, 115020 (2010).
 - [50] B. Fuks and R. Ruiz, A comprehensive framework for studying W' and Z' bosons at hadron colliders with automated jet veto resummation, *JHEP* **05**, 032 (2017).
 - [51] G. C. Branco and M. N. Rebelo, New Physics in the Flavour Sector in the presence of Flavour Changing Neutral Currents, *PoS Corfu2012*, 024 (2013).
 - [52] K. S. Babu, J. Julio, and Y. Zhang, Perturbative unitarity constraints on general W' models and collider implications, *Nucl. Phys. B* **858**, 468 (2012).
 - [53] M. Jacob and G. C. Wick, On the General Theory of Collisions for Particles with Spin, *Annals Phys.* **7**, 404 (1959).
 - [54] U. Baur and D. Zeppenfeld, Unitarity Constraints on the Electroweak Three Vector Boson Vertices, *Phys. Lett. B* **201**, 383 (1988).
 - [55] T. Corbett, O. J. P. Eboli, and M. C. Gonzalez-Garcia, Unitarity Constraints on Dimension-Six Operators, *Phys. Rev. D* **91**, 035014 (2015).
 - [56] Q. Fu, J. C. Yang, C. X. Yue, and Y. C. Guo, The study of neutral triple gauge couplings in the process $e^+e^- \rightarrow Z\gamma$ including unitarity bounds, *Nucl. Phys. B* **972**, 115543 (2021).
 - [57] J. C. Romao and J. P. Silva, A resource for signs and Feynman diagrams of the Standard Model, *Int. J. Mod. Phys. A* **27**, 1230025 (2012).

- [58] LEP, A Combination of preliminary electroweak measurements and constraints on the standard model (2003), [arXiv:hep-ex/0312023](#).
- [59] V. Khachatryan *et al.* (CMS), Evidence for exclusive $\gamma\gamma \rightarrow W^+W^-$ production and constraints on anomalous quartic gauge couplings in pp collisions at $\sqrt{s} = 7$ and 8 TeV, [JHEP **08**, 119 \(2016\)](#).
- [60] M. Rauch, Vector-Boson Fusion and Vector-Boson Scattering, [arXiv:1610.08420](#).
- [61] D. R. Green, P. Meade, and M. A. Pleier, Multiboson interactions at the LHC, [Rev. Mod. Phys. **89**, 035008 \(2017\)](#).
- [62] I. A. Serenkova, P. Osland, and A. A. Pankov, Improved bounds on $W - W'$ mixing with ATLAS resonant WZ production data at the LHC at $\sqrt{s} = 13$ TeV, [Phys. Rev. D **100**, 015007 \(2019\)](#).
- [63] J. Fuentes-Martin, A. Greljo, J. M. Camalich, and J. D. Ruiz-Alvarez, Charm physics confronts high- p_T lepton tails, [JHEP **11**, 080 \(2020\)](#).
- [64] A. Alloul, N. D. Christensen, C. Degrande, C. Duhr, and B. Fuks, FeynRules 2.0 - A complete toolbox for tree-level phenomenology, [Comput. Phys. Commun. **185**, 2250 \(2014\)](#).
- [65] N. D. Christensen and C. Duhr, FeynRules - Feynman rules made easy, [Comput. Phys. Commun. **180**, 1614 \(2009\)](#).
- [66] C. Degrande, C. Duhr, B. Fuks, D. Grellscheid, O. Mattelaer, and T. Reiter, UFO - The Universal FeynRules Output, [Comput. Phys. Commun. **183**, 1201 \(2012\)](#).
- [67] J. Alwall, R. Frederix, S. Frixione, V. Hirschi, F. Maltoni, O. Mattelaer, H. S. Shao, T. Stelzer, P. Torrielli, and M. Zaro, The automated computation of tree-level and next-to-leading order differential cross sections, and their matching to parton shower simulations, [JHEP **07**, 079 \(2014\)](#).
- [68] T. Sjöstrand, S. Ask, J. R. Christiansen, R. Corke, N. Desai, P. Ilten, S. Mrenna, S. Prestel, C. O. Rasmussen, and P. Z. Skands, An introduction to PYTHIA 8.2, [Comput. Phys. Commun. **191**, 159 \(2015\)](#).
- [69] J. Favereau, C. Delaere, P. Demin, A. Giammanco, V. Lemaître, A. Mertens, and M. Selvaggi (DELPHES 3), DELPHES 3, A modular framework for fast simulation of a generic collider experiment, [JHEP **02**, 057 \(2014\)](#).
- [70] R. D. Ball, V. Bertone, F. Cerutti, L. D. Debbio, S. Forte, A. Guffanti, J. I. Latorre, J. Rojo, and M. Ubiali, Impact of Heavy Quark Masses on Parton Distributions and LHC Phenomenol-

- ogy, *Nucl. Phys. B* **849**, 296 (2011).
- [71] R. D. Ball *et al.*, Parton distributions with LHC data, *Nucl. Phys. B* **867**, 244 (2013).
- [72] E. Conte, B. Fuks, and G. Serret, MadAnalysis 5, A User-Friendly Framework for Collider Phenomenology, *Comput. Phys. Commun.* **184**, 222 (2013).
- [73] G. Altarelli, B. Mele, and M. Ruiz-Altaba, Searching for New Heavy Vector Bosons in $p\bar{p}$ Colliders, *Z. Phys. C* **45**, 109 (1989), [Erratum: *Z.Phys.C* 47, 676 (1990)].
- [74] S. Jezequel (ATLAS, CMS), Prospects for the high-luminosity LHC, *Nucl. Phys. B Proc. Suppl.* **245**, 145 (2013).
- [75] C. Henderson (CMS), Future Physics Prospects with the CMS Detector at the High-Luminosity LHC, *SciPost Phys.Proc.* **111**, 8 (2022).
- [76] C. O. Dib, C. S. Kim, K. Wang, and J. Zhang, Distinguishing Dirac/Majorana Sterile Neutrinos at the LHC, *Phys. Rev. D* **94**, 013005 (2016).
- [77] C. X. Yue and X. J. Cheng, Constraints on the charged-current non-standard neutrino interactions induced by the gauge boson W' , *Nucl. Phys. B* **963**, 115280 (2021).

Appendix A

With the help of Eq. (6), the amplitudes corresponding to the Feynman diagrams in Fig. 1 can be written as

$$\begin{aligned}
\mathcal{M}\left(u_{-\frac{1}{2}}\bar{d}_{\frac{1}{2}}\rightarrow W_0^+Z_0\right) &= g^2|V_{ud}|^2A_L^{ud}c_W\frac{(2M_{W'}^2+M_Z^2)}{2M_{W'}M_Z}e^{-i\phi}\sin\theta+\mathcal{O}(s^{-1}), \\
\mathcal{M}\left(d_{-\frac{1}{2}}\bar{u}_{\frac{1}{2}}\rightarrow W_0^-Z_0\right) &= g^2|V_{ud}|^2A_L^{ud*}c_W\frac{(2M_{W'}^2+M_Z^2)}{2M_{W'}M_Z}e^{-i\phi}\sin\theta+\mathcal{O}(s^{-1}), \\
\mathcal{M}\left(u_{-\frac{1}{2}}\bar{u}_{\frac{1}{2}}\rightarrow W_0^+W_0^-\right) &= -\left[g^2|V_{ud}|^2|A_L^{ud}|^2-\left(\frac{1}{2}-\frac{2}{3}s_W^2\right)\frac{g^2|V_{ud}|^2M_Z^2}{2M_{W'}^2}\right. \\
&\quad \left.-\frac{g^2|V_{ud}|^2(|A_L^{ud}|^2-1)M_{Z'}^2}{4M_{W'}^2}\right]e^{-i\phi}\sin\theta+\mathcal{O}(s^{-1}), \\
\mathcal{M}\left(d_{-\frac{1}{2}}\bar{d}_{\frac{1}{2}}\rightarrow W_0^+W_0^-\right) &= \left[g^2|V_{ud}|^2|A_L^{ud}|^2+\left(\frac{1}{3}s_W^2-\frac{1}{2}\right)\frac{g^2|V_{ud}|^2M_Z^2}{2M_{W'}^2}\right. \\
&\quad \left.-\frac{g^2|V_{ud}|^2(|A_L^{ud}|^2-1)M_{Z'}^2}{4M_{W'}^2}\right]e^{-i\phi}\sin\theta+\mathcal{O}(s^{-1}), \\
\mathcal{M}\left(u_{-\frac{1}{2}}\bar{u}_{\frac{1}{2}}\rightarrow W_0^+W_0^-\right) &= \mathcal{M}\left(-d_{\frac{1}{2}}\bar{d}_{\frac{1}{2}}\rightarrow W_0^+W_0^-\right)
\end{aligned}$$

$$\begin{aligned}
&= \pm g^2 |V_{ud}|^2 A_L^{ud} \left[\frac{(M_{W'}^2 + M_W^2)}{2M_{W'}M_W} - \frac{M_{Z'}^2}{4M_{W'}M_W} \right] e^{-i\phi} \sin \theta + \mathcal{O}(s^{-1}), \\
\mathcal{M} \left(u_{-\frac{1}{2}} \bar{u}_{\frac{1}{2}} \rightarrow W_0'^- W_0^+ \right) &= \mathcal{M} \left(-d_{\frac{1}{2}} \bar{d}_{\frac{1}{2}} \rightarrow W_0'^- W_0^+ \right) \\
&= \pm g^2 |V_{ud}|^2 A_L^{ud*} \left[\frac{(M_{W'}^2 + M_W^2)}{2M_{W'}M_W} + \frac{M_{Z'}^2}{4M_{W'}M_W} \right] e^{-i\phi} \sin \theta + \mathcal{O}(s^{-1}), \\
\mathcal{M} \left(u_{\frac{1}{2}} \bar{d}_{-\frac{1}{2}} \rightarrow W_0'^+ Z_0 \right) &= -g^2 |V_{ud}|^2 A_R^{ud} s_W^2 \frac{(2M_{W'}^2 + M_Z^2)}{2c_W M_{W'} M_Z} e^{i\phi} \sin \theta + \mathcal{O}(s^{-1}), \\
\mathcal{M} \left(d_{\frac{1}{2}} \bar{u}_{-\frac{1}{2}} \rightarrow W_0'^- Z_0 \right) &= -g^2 |V_{ud}|^2 A_R^{ud*} s_W^2 \frac{(2M_{W'}^2 + M_Z^2)}{2c_W M_{W'} M_Z} e^{i\phi} \sin \theta + \mathcal{O}(s^{-1}), \\
\mathcal{M} \left(u_{\frac{1}{2}} \bar{u}_{-\frac{1}{2}} \rightarrow W_0'^+ W_0'^- \right) &= - \left[g^2 |V_{ud}|^2 |A_R^{ud}|^2 - \frac{g^2 |V_{ud}|^2 s_W^4 M_Z^2}{3c_W^2 M_{W'}^2} \right. \\
&\quad \left. - \left(\frac{|A_R^{ud}|^2}{2} - \frac{2s_W^2}{3c_W^2} \right) \frac{g^2 |V_{ud}|^2 M_{Z'}^2}{2M_{W'}^2} \right] e^{i\phi} \sin \theta + \mathcal{O}(s^{-1}), \\
\mathcal{M} \left(d_{\frac{1}{2}} \bar{d}_{-\frac{1}{2}} \rightarrow W_0'^+ W_0'^- \right) &= \left[g^2 |V_{ud}|^2 |A_R^{ud}|^2 - \frac{g^2 |V_{ud}|^2 s_W^4 M_Z^2}{6c_W^2 M_{W'}^2} \right. \\
&\quad \left. + \left(\frac{s_W^2}{3c_W^2} - \frac{|A_R^{ud}|^2}{2} \right) \frac{g^2 |V_{ud}|^2 M_{Z'}^2}{2M_{W'}^2} \right] e^{i\phi} \sin \theta + \mathcal{O}(s^{-1}).
\end{aligned}$$

$$\begin{aligned}
\mathcal{M} \left(e_{-\frac{1}{2}}^- e_{\frac{1}{2}}^+ \rightarrow W_0'^+ W_0'^- \right) &= \mathcal{M} \left(\mu_{-\frac{1}{2}}^+ \mu_{\frac{1}{2}}^- \rightarrow W_0'^+ W_0'^- \right) \\
&= \left[g^2 |B_L^{ee}|^2 + \left(s_W^2 - \frac{1}{2} \right) \frac{g^2 M_Z^2}{2M_{W'}^2} - \frac{(|B_L^{ee}|^2 - 1) g^2 M_{Z'}^2}{4M_{W'}^2} \right] e^{-i\phi} \sin \theta + \mathcal{O}(s^{-1}), \\
\mathcal{M} \left(e_{-\frac{1}{2}}^- e_{\frac{1}{2}}^+ \rightarrow W_0'^+ W_0^- \right) &= \mathcal{M} \left(\mu_{-\frac{1}{2}}^+ \mu_{\frac{1}{2}}^- \rightarrow W_0'^+ W_0^- \right) \\
&= g^2 B_L^{ee*} \frac{2(M_{W'}^2 + M_W^2) - M_{Z'}^2}{4M_{W'}M_W} e^{-i\phi} \sin \theta + \mathcal{O}(s^{-1}), \\
\mathcal{M} \left(e_{-\frac{1}{2}}^- e_{\frac{1}{2}}^+ \rightarrow W_0'^- W_0^+ \right) &= \mathcal{M} \left(\mu_{-\frac{1}{2}}^+ \mu_{\frac{1}{2}}^- \rightarrow W_0'^- W_0^+ \right) \\
&= -g^2 B_L^{ee} \frac{2(M_{W'}^2 + M_W^2) + M_{Z'}^2}{4M_{W'}M_W} e^{-i\phi} \sin \theta + \mathcal{O}(s^{-1}), \\
\mathcal{M} \left(e_{-\frac{1}{2}}^- \mu_{\frac{1}{2}}^- \rightarrow W_0'^+ W_0'^- \right) &= \mathcal{M} \left(\mu_{-\frac{1}{2}}^+ e_{\frac{1}{2}}^+ \rightarrow W_0'^+ W_0'^- \right) = 2g^2 |B_L^{ee}|^2 e^{-i\phi} \sin \theta + \mathcal{O}(s^{-1}), \\
\mathcal{M} \left(e_{-\frac{1}{2}}^- \mu_{\frac{1}{2}}^- \rightarrow W_0'^+ W_0^- \right) &= \mathcal{M} \left(\mu_{-\frac{1}{2}}^+ e_{\frac{1}{2}}^+ \rightarrow W_0'^+ W_0^- \right) \\
&= g^2 B_R^{ee*} \frac{M_{W'}^2 + M_W^2}{2M_{W'}M_W} e^{-i\phi} \sin \theta + \mathcal{O}(s^{-1}), \\
\mathcal{M} \left(e_{-\frac{1}{2}}^- \mu_{\frac{1}{2}}^- \rightarrow W_0'^- W_0^+ \right) &= \mathcal{M} \left(\mu_{-\frac{1}{2}}^+ e_{\frac{1}{2}}^+ \rightarrow W_0'^- W_0^+ \right) \\
&= -g^2 B_L^{ee} \frac{M_{W'}^2 + M_W^2}{2M_{W'}M_W} e^{-i\phi} \sin \theta + \mathcal{O}(s^{-1}),
\end{aligned}$$

$$\begin{aligned}
\mathcal{M}\left(e_{-\frac{1}{2}}^-\bar{\nu}_e \rightarrow W_0'^- Z_0\right) &= -\frac{g^2 B_L^{ee} c_W M_Z}{2M_{W'}} e^{-i\phi} \sin\theta + \mathcal{O}(s^{-1}), \\
\mathcal{M}\left(\nu_e e_{\frac{1}{2}}^+ \rightarrow W_0'^+ Z_0\right) &= \frac{g^2 B_L^{ee*} c_W (2M_{W'}^2 + M_Z^2)}{2M_{W'} M_Z} e^{-i\phi} \sin\theta + \mathcal{O}(s^{-1}).
\end{aligned} \tag{A.1}$$

$\mathcal{O}(s^{-1})$ indicates higher order terms. It is small and ignored in this study.

Using the relationship $|T_J| \leq 1$, we can obtain a constraint on $A_Y^{qq'}$ or $B_L^{\alpha\alpha}$ from each of the above processes. All of these constraints should be satisfied; therefore, we concentrate on the tightest ones, which depend on the free parameters $M_{W'}$ and $M_{Z'}$. In the case of $0.2 \text{ TeV} < M_{Z'} < 2 \text{ TeV}$ [25] and $s \rightarrow \infty$, the tightest bounds are given by

$$\begin{aligned}
A_L^{ud}\left(u_{-\frac{1}{2}}\bar{d}_{\frac{1}{2}} \rightarrow W_0'^+ Z_0\right) &= A_L^{ud*}\left(d_{-\frac{1}{2}}\bar{u}_{\frac{1}{2}} \rightarrow W_0'^- Z_0\right) < \frac{24\sqrt{2}\pi M_{W'} M_Z}{g^2 |V_{ud}|^2 c_W (2M_{W'}^2 + M_Z^2)}, \\
A_L^{ud}\left(u_{-\frac{1}{2}}\bar{u}_{\frac{1}{2}} \rightarrow W_0'^+ W_0'^-\right) &< \sqrt{\frac{48\sqrt{2}\pi M_{W'}^2 - g^2 |V_{ud}|^2 M_Z^2 + g^2 |V_{ud}|^2 M_{Z'}^2}{g^2 |V_{ud}|^2 |M_{Z'}^2 - 4M_{W'}^2|} + \frac{4s_W^2 M_Z^2}{3|M_{Z'}^2 - 4M_{W'}^2|}}, \\
A_L^{ud*}\left(u_{-\frac{1}{2}}\bar{u}_{\frac{1}{2}} \rightarrow W_0'^- W_0'^+\right) &= A_L^{ud*}\left(d_{-\frac{1}{2}}\bar{d}_{\frac{1}{2}} \rightarrow W_0'^- W_0'^+\right) < \frac{48\pi M_{W'} M_W}{g^2 |V_{ud}|^2 (2M_{W'}^2 + 2M_W^2 + M_{Z'}^2)}, \\
A_R^{ud}\left(u_{\frac{1}{2}}\bar{d}_{-\frac{1}{2}} \rightarrow W_0'^+ Z_0\right) &= A_R^{ud*}\left(d_{\frac{1}{2}}\bar{u}_{-\frac{1}{2}} \rightarrow W_0'^- Z_0\right) < \frac{24\sqrt{2}\pi c_W M_{W'} M_Z}{g^2 |V_{ud}|^2 s_W^2 (2M_{W'}^2 + M_Z^2)}, \\
A_R^{ud}\left(d_{\frac{1}{2}}\bar{d}_{-\frac{1}{2}} \rightarrow W_0'^+ W_0'^-\right) &< \sqrt{\frac{48\sqrt{2}\pi M_{W'}^2}{g^2 |V_{ud}|^2 (4M_{W'}^2 - M_{Z'}^2)} + \frac{2s_W^2 (s_W^2 M_Z^2 - M_{Z'}^2)}{3c_W^2 (4M_{W'}^2 - M_{Z'}^2)}}, \\
B_L^{ee}\left(e_{-\frac{1}{2}}^- e_{\frac{1}{2}}^+ \rightarrow W_0'^- W_0'^+\right) &< \frac{48\sqrt{2}\pi M_{W'} M_W}{2g^2 (M_{W'}^2 + M_W^2) + g^2 M_{Z'}^2}, \\
B_L^{ee}\left(e_{-\frac{1}{2}}^- \mu_{\frac{1}{2}}^- \rightarrow W_0'^+ W_0'^-\right) &= B_L^{ee}\left(\mu_{-\frac{1}{2}}^+ e_{\frac{1}{2}}^+ \rightarrow W_0'^+ W_0'^-\right) < \sqrt{\frac{6\sqrt{2}\pi}{g^2}}, \\
B_L^{ee*}\left(\nu_e e_{\frac{1}{2}}^+ \rightarrow W_0'^+ Z_0\right) &< \frac{24\sqrt{2}\pi M_{W'} M_Z}{g^2 c_W (2M_{W'}^2 + M_Z^2)}.
\end{aligned} \tag{A.2}$$

The relationship between $M_{W'}$ and the coupling parameters according to Eq. (A.2) are shown in Fig. 17.

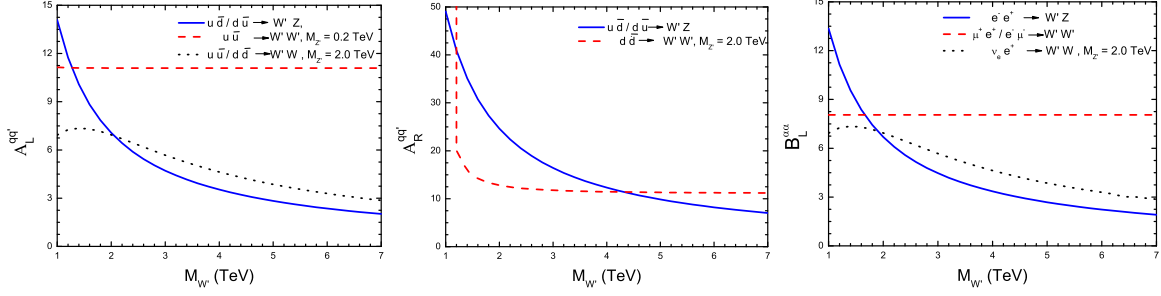


FIG. 17. Tightest constraints on the coupling parameters $A_Y^{qq'}$ and $B_L^{\alpha\alpha}$ as functions of $M_{W'}$.

For a wide range of $M_{W'}$, the tightest bound on $A_L^{qq'}$ originates from the process $u\bar{d} (d\bar{u}) \rightarrow W'Z$. Similarly, the tightest bound on $B_L^{\alpha\alpha}$ mainly arises from the process $e^-e^+ \rightarrow W'Z$. For simplicity, we only use the above bounds. For $A_R^{qq'}$, the two tightest bounds (depending on $M_{W'}$) are both considered.